Inorganic Chemistry
Article

Inorg. Chem. **2010**, *49*, 7861–7879 **7861**
DOI: 10.1021/ic100760t

Preparation and Characterization of $(CNSSS)_2(A)_2$ ($A = AsF_6^-$, SbF_6^-, $Sb_2F_{11}^-$) Containing the O_2-like 5,5′-Bis(1,2,3,4-trithiazolium) Dication: The Second Example of a Simple Nonsterically Hindered Main-Group Diradical That Retains Its Paramagnetism in the Solid State

T. Stanley Cameron,[†] Andreas Decken,[‡] Friedrich Grein,[‡] Carsten Knapp,[‡,§] Jack Passmore,[*,‡] J. Mikko Rautiainen,[‡] Konstantin V. Shuvaev,[‡,⊥] Robert C. Thompson,[¶] and Dale J. Wood[‡,∥]

[†] *Department of Chemistry, Dalhousie University, Halifax, Nova Scotia B3H 4J3, Canada,* [‡] *Department of Chemistry, University of New Brunswick, Fredericton, New Brunswick E3B 5A3, Canada, and* [¶] *Department of Chemistry, University of British Columbia, Vancouver, British Columbia V6T 1Z1, Canada.* [§] *Current address: Institut für Anorganische and Analytische Chemie, Albert-Ludwigs-Universität Freiburg, Albertstrasse 21, 79104 Freiburg im Breisgau, Germany.* [⊥] *Current address: Department of Chemistry, Memorial University of Newfoundland, St. John's A1B 3X7, Canada.* [∥] *Current address: Department of Chemistry, Bishop's University, 2600 College Street, Sherbrooke, Québec J1M 1Z7, Canada.*

Received April 20, 2010

The reaction of NC−CN with a 1:1 mixture of $S_4(MF_6)_2$ and $S_8(MF_6)_2$ (M = As, Sb) (stoichiometrically equivalent to four "S_3MF_6" units) results in the quantitative formation of $S_3NCCNS_3(MF_6)_2$ [**7**$(MF_6)_2$], which is the thermodynamic sink in this reaction. The $Sb_2F_{11}^-$ salt **7**$(Sb_2F_{11})_2$ is prepared by the addition of an excess of SbF_5 to **7**$(AsF_6)_2$. Crystal structure determinations for all three salts show that $\mathbf{7}^{2+}$ can be viewed as two R-CNS_3^+ radical cations joined together by a C−C single bond. The two rings are coplanar and in a trans orientation due to electrostatic $N^{\delta-}\cdots S^{\delta+}$ interactions. The classically bonded alternative (quinoidal structure), in which the octet rule is obeyed, is not observed and is much higher in energy based on calculated estimates and a simple comparison of π bond energies. Calculated molecular orbitals (MOs) support this, showing that the MO corresponding to the quinoidal structure lies higher in energy than the nearly degenerate singly occupied MOs of $\mathbf{7}^{2+}$. The vibrational spectra of $\mathbf{7}^{2+}$ in all salts were assigned based on a normal-coordinate analysis and theoretical vibrational frequencies calculated at the PBE0/6-31G* level. In the solid state, $\mathbf{7}^{2+}$ is a planar disjoint diradical with essentially degenerate open-shell singlet and triplet states. The disjoint nature of the diradical cation $\mathbf{7}^{2+}$ is established by magnetic susceptibility studies of the $Sb_2F_{11}^-$ salt doped in an isomorphous diamagnetic host material $(CNSNS)_2(Sb_2F_{11})_2$ [**10**$(Sb_2F_{11})_2$]. *Intra*molecular spin coupling is extremely weak corresponding to a singlet−triplet gap ($\Delta E_{ST} = 2J$) of $<\pm 2$ cm^{-1}. CASPT2[12,12]/6-311G* calculations support a triplet ground state with a small singlet−triplet gap. The single-crystal electron paramagnetic resonance (EPR) of **7**$(Sb_2F_{11})_2$ doped in **10**$(Sb_2F_{11})_2$ is in agreement with the triplet state arising from the weak coupling between the unpaired electrons residing in p_π orbitals in each of the rings. Variable-temperature susceptibility data for bulk samples of **7**$(A)_2$ ($A = SbF_6^-$, AsF_6^-, $Sb_2F_{11}^-$) are analyzed by employing both 1D chain and 2D sheet magnetic models. These studies reveal significant *inter*molecular exchange approximating that of a 1D chain for the SbF_6^- salt with $|J| = 32$ cm^{-1}. The exchange coupling is on the same order of magnitude as that for the AsF_6^- salt, although in this case it is likely that there are complex exchange pathways where no particular one is dominant. *Inter*molecular exchange in the $Sb_2F_{11}^-$ salt is an order of magnitude weaker. In solution, the EPR spectrum of $\mathbf{7}^{2+}$ shows a broad triplet resonance as well as a sharp resonance that is tentatively attributed to a rotomer of the $\mathbf{7}^{2+}$/anion pair, which is likely the origin of the green species given on dissolution of the red $\mathbf{7}^{2+}$ salts in $SO_2/AsF_3/MF_5$. We account for the many similarities between O_2 and $\mathbf{7}^{2+}$, which are the only simple nonsterically hindered nonmetal diradicals to retain their paramagnetism in the solid state. $\mathbf{7}^{2+}$ is also the first isolable, essentially sulfur-based diradical as evidenced by calculated spin densities.

1. Introduction

We have shown previously that the reaction of nitriles R—C≡N with a mixture of $S_4(AsF_6)_2$ and $S_8(AsF_6)_2$ gave the AsF_6^- salts of stable 7π radical cations $RCNSSS^{\bullet+}$ [$\mathbf{1}^{\bullet+}$; R = F_3C,[1] Cl_3C,[2] F_5C_2,[2] Cl,[3a] Br,[3a] I,[3a]

*To whom correspondence should be addressed. E-mail: passmore@unb.ca. Tel: 1-506-453-4821. Fax: 1-506-453-4981.

(1) Cameron, T. S.; Haddon, R. C.; Mattar, S. M.; Parsons, S.; Passmore, J. *Inorg. Chem.* **1992**, *31*, 2274.
(2) Decken, A.; Mattar, S. M.; Passmore, J.; Shuvaev, K. V.; Thompson, L. T. *Inorg. Chem.* **2006**, *45*, 3878.

Published on Web 08/10/2010

Chart 1

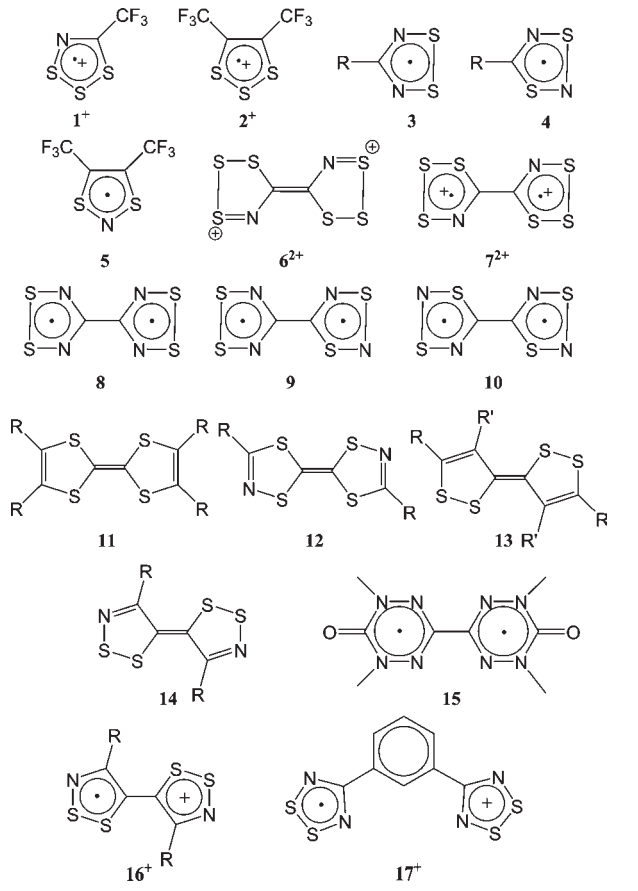

$C_2F_4(CNSSS^{\bullet+})$,[3b] $C_4F_8(CNSSS^{\bullet+})$,[3b] $C_3F_6(CNSSS^{\bullet+})$[3b]] in high yields (eq 1).

$$RCN + 1/4\ S_4(AsF_6)_2 + 1/4\ S_8(AsF_6)_2 \xrightarrow{SO_2} \mathbf{1}^{+\bullet}\,AsF_6^- \qquad (1)$$

These molecules and $\mathbf{2}^+$ (Chart 1) are members of a unique class of stable, essentially sulfur-based main-group 7π radicals and adopt a variety of solid-state structures ranging from nearly diamagnetic dimers (e.g., R = Cl, Br, I),[3a] with thermally accessible triplet states detected by electron paramagnetic resonance (EPR) to paramagnetic weakly coupled 1D chains (R = CF_3, CCl_3, C_2F_5).[1,2] Of these, the diradical $(CNSSS^{\bullet+})_2$, $\mathbf{7}^{2+}$, reported by us in a series of preliminary accounts,[4] is particularly interesting. All salts of $\mathbf{7}^{2+}$ are paramagnetic, containing two unpaired electrons with only weak *anti*ferromagnetic *intra*molecular coupling,[4c] and $\mathbf{7}^{2+}$ in its various salts is the first example (other than O_2[5]) of a simple nonsterically hindered main-group diradical to retain its bulk paramagnetism in the solid state and to resemble O_2 in many ways.

The diradical $\mathbf{7}^{2+}$ does not adopt the expected classically bonded alternative (i.e., $\mathbf{6}^{2+}$) in which the Lewis octet rule is obeyed but rather contains two unpaired electrons per molecule in the nonclassically bonded diradical structure $\mathbf{7}^{2+}$. The related main-group diradicals **8**,[6] **9**,[7] and **10**[8] (Chart 1) also do not adopt the expected quinoidal structures (e.g., those given in Chart 2 of ref 9), contrary to the situation observed for **11**−**14** (Chart 1) and other related molecules.[10] $\mathbf{7}^{2+}$, **8**, **9**, and **10** are members of a small subclass of isolable nonsterically hindered main-group diradicals that are unique in that they contain two radical rings joined by two atoms and yet do not adopt classical Lewis structures. However, all salts of $\mathbf{7}^{2+}$ are paramagnetic in the solid state, whereas the neutral diradicals **8** and **9** dimerize via $\pi^*-\pi^*$ interaction and thus are diamagnetic. A crystal structure of **10** was not obtained, but the evidence implies that it exists in two forms, one paramagnetic and the other diamagnetic, which becomes paramagnetic upon grinding.[8] The 1,1′,5,5′-tetramethyl-6,6′-dioxo-3,3′-biverdazyl (**15**) is diamagnetic as a result of substantial *intra*molecular *anti*ferromagnetic coupling of the unpaired electrons on each of the rings, leading to a singlet ground state (singlet−triplet gap = $-760\ cm^{-1}$).[11] Selected other classes of diradicals include dinitroxides,[12] triphenylmethyl diradicals,[13] and other organic framework-based

(3) (a) Cameron, T. S.; Decken, A.; Kowalczyk, R. M.; McInnes, E. J. L.; Passmore, J.; Rawson, J. M.; Shuvaev, K. V.; Thompson, L. K. *Chem. Commun*. **2006**, 2277. (b) Decken, A.; Ebdah, M.; Kowalczyk, R. M.; Landee, C. P.; McInnes, E. J. L.; Passmore, J.; Shuvaev, K. V.; Thompson, L. K. *Inorg. Chem*. **2007**, *46*, 7756.

(4) (a) Boyle, P. D.; Parsons, S.; Passmore, J.; Wood, D. J. *J. Chem. Soc., Chem. Commun*. **1993**, 199. *J. Chem. Soc., Chem. Commun*. **1994**, 676. (b) Boyle, P. D.; Passmore, J.; Wood, D. J. *Phosphorus, Sulfur, Silicon* **1994**, *93*−*94*, 227. (c) Enright, G. D.; Morton, J. R.; Passmore, J.; Preston, K. F.; Thompson, R. C.; Wood, D. J. *J. Chem. Soc., Chem. Commun*. **1996**, 967. (d) Berces, A.; Enright, G. D.; Morton, J. R.; Passmore, J.; Preston, K. F.; Thompson, R. C.; Wood, D. J. *Phosphorus, Sulfur, Silicon* **1997**, *124*−*125*, 331. (e) Boyle, P. D.; Cameron, T. S.; Decken, A.; Passmore, J.; Wood, D. J. *Phosphorus, Sulfur, Silicon* **1997**, *124*−*125*, 549. (f) Berces, A.; Enright, G. D.; Mclaurin, G. E.; Morton, J. R.; Preston, K. F.; Passmore, J.; Wood, D. J. *Magn. Reson. Chem*. **1999**, *37*, 353.

(5) (a) To date six different phases of solid oxygen are known to exist. At normal pressures, three phases exist. The α and β phases show antiferromagnetic behavior. The α phase exhibits long-range magnetic ordering, while only short-range magnetic ordering is observed in the β phase. The γ phase is paramagnetic. There is no conclusive evidence of the magnetic behavior of the high-pressure phases $\delta-\zeta$ of oxygen. However, it is believed that the δ phase behaves similarly to the α phase and that the ε and ζ phases are nonmagnetic because of magnetic collapse. (b) See: Freiman, Y. A.; Jodl, H. J. *Phys. Rep*. **2004**, *401*, 1 and references cited therein.

(6) (a) Bryan, C. D.; Cordes, A. W.; Haddon, R. C.; Hicks, R. G.; Oakley, R. T.; Palstra, T. T. M.; Perel, A. J. *J. Chem. Soc., Chem. Commun*. **1994**, 1447. (b) Bryan, C. D.; Cordes, A. W.; Goddard, J. D.; Haddon, R. C.; Hicks, R. G.; MacKinnon, C. D.; Mawhinney, R. C.; Oakley, R. T.; Palstra, T. T. M.; Perel, A. J. *J. Am. Chem. Soc*. **1996**, *118*, 330.

(7) (a) Cameron, T. S.; Lemaire, M. T.; Passmore, J.; Rawson, J. M.; Shuvaev, K. V.; Thompson, L. K. *Inorg. Chem*. **2005**, *44*, 2576. (b) Decken, A.; Cameron, T. S.; Passmore, J.; Rautiainen, J. M.; Reed, R. W.; Shuvaev, K. V.; Thompson, L. K. *Inorg. Chem*. **2007**, *46*, 7436.

(8) Antorrena, G.; Brownridge, S.; Cameron, T. S.; Palacio, F.; Parsons, S.; Passmore, J.; Thompson, L. K.; Zarlaida, F. *Can. J. Chem*. **2002**, *80*, 1568.

(9) Parsons, S.; Passmore, J.; White, P. S. *J. Chem. Soc., Dalton Trans*. **1993**, 1499.

(10) (a) Barclay, T. M.; Cordes, A. W.; Oakley, R. T.; Preuss, K. E.; Reed, R. W. *Chem. Commun*. **1998**, 1039. (b) Barclay, T. M.; Beer, L.; Cordes, A. W.; Haddon, R. C.; Itkis, M. I.; Oakley, R. T.; Preuss, K. E.; Reed, R. W. *J. Am. Chem. Soc*. **1999**, *121*, 6657. (c) Ellern, A.; Bernstein, J.; Becker, J. Y.; Zamir, S.; Shahal, L.; Cohen, S. *Chem. Mater*. **1994**, *6*, 1378. (d) Oakley, R. T.; Richardson, J. F.; v. H. Spence, R. E. *J. Chem. Soc., Chem. Commun*. **1993**, 1226. (e) Oakley, R. T.; Richardson, J. F.; v. H. Spence, R. E. *J. Org. Chem*. **1994**, *59*, 2997. (f) Chu, S.-L.; Wai, K.-F.; Lai, T.-F.; Sammes, M. P. *Tetrahedron. Lett*. **1993**, *34*, 847. (g) Behringer, H.; Meinetsberger, E. *Liebigs Ann. Chem*. **1981**, 1928.

(11) (a) Brook, D. J. R.; Fox, H. H.; Lynch, V.; Fox, M. A. *J. Phys. Chem*. **1996**, *100*, 2066. (b) Green, M. T.; McCornick, T. A. *Inorg. Chem*. **1999**, *38*, 3061.

(12) (a) Matsumoto, T.; Koga, N.; Iwamura, H. *J. Am. Chem. Soc*. **1992**, *114*, 5448. (b) Hernàndez-Gasio, E.; Mas, M.; Molins, E.; Rovira, C.; Veciana, J.; Borrás-Almenar, J. J.; Coronado, E. *Chem. Mater*. **1994**, *6*, 2398. (c) Frank, N. L.; Clérac, R.; Sutter, J.-P.; Daro, N.; Kahn, O.; Coulon, C.; Green, M. T.; Golhen, S.; Ouahab, L. *J. Am. Chem. Soc*. **2000**, *122*, 2053. (d) Wautelet, P.; Le Moigne, J.; Videva, V.; Turek, P. *J. Org. Chem*. **2003**, *68*, 8025.

compounds.[14] These and other related organic/main-group diradicals and diradicaloids[15−17] are not included in this subclass because they do not conform to the aforementioned criteria (i.e., the direct connection of sterically nonhindered radical centers by two atoms).[18] Salts of $\mathbf{7}^{2+}$ contain the first examples of stable, isolable, almost completely sulfur-based diradicals.

In this paper, we give a full account of the preparation of $\mathbf{7}(A)_2$ [A = AsF_6^-, SbF_6^-, $Sb_2F_{11}^-$] salts, their vibrational spectra, structures, a variable-temperature magnetic study of solid $\mathbf{7}(Sb_2F_{11})_2$ imbedded in a matrix of the isostructural $\mathbf{10}(Sb_2F_{11})_2$, and the electronic structure of $\mathbf{7}^{2+}$ with focus on the characterization of $\mathbf{7}^{2+}$ in the gas, solution, and solid states as a molecular species, and we account for the remarkable similarities between it and O_2 (see Figure 11). Parts of this work were reported in 1993 and 1996 as preliminary communications[4a,c] and later as three extended abstracts of conference presentations.[4b,d,e] A single-crystal EPR study of $\mathbf{7}(Sb_2F_{11})_2$ in a matrix of the diamagnetic isostructural $\mathbf{10}(Sb_2F_{11})_2$ was published in *J. Magn. Reson. Chem.* in 1999.[4f] However, numerous problems and questions remained. The present, much more complete understanding of the system was aided by a variable-temperature magnetic study of the crystalline $\mathbf{7}(Sb_2F_{11})_2$ in a matrix of the diamagnetic isostructural $\mathbf{10}(Sb_2F_{11})_2$, which experimentally established the triplet and singlet states to be identical in energy ± 2 cm^{-1}. This simplified the analysis of the variable-temperature magnetic data on $\mathbf{7}(SbF_6)_2$ and led to a reinterpretation of the previously published data on $\mathbf{7}(AsF_6)_2$ and $\mathbf{7}(Sb_2F_{11})_2$.[4c] Only in recent years have theoretical calculations that permit the prediction of the lowest states of $\mathbf{7}^{2+}$ and vibrational spectra in agreement with the experimental results become feasible. This has allowed us to apply theoretical methods to better understand $\mathbf{7}^{2+}$ in the gaseous, solution, and solid phases. $\mathbf{7}^{2+}$ had been previously analyzed by Genin and Hoffmann[19] using extended Hückel calculations describing $\mathbf{7}^{2+}$ and related species as models for a ferromagnetic polymer. Some of the earlier experimental work has been repeated, including the crystal structure of $\mathbf{7}(SbF_6)_2$ and red $\mathbf{7}(Sb_2F_{11})_2$ using modern state-of-the-art variable-temperature X-ray methods, leading us to conclude that the structures of the red and green crystals of $\mathbf{7}(Sb_2F_{11})_2$ are likely the same, in contrast to previous claims that they are different.[4e,20] Variable-temperature solid-state magnetic studies and other bulk physical properties on single crystals of $\mathbf{7}(MF_6)_2$ will be the subject of a separate publication.[21]

2. Experimental Section

2.1. Materials. The preparation of $\mathbf{10}(AsF_6)_2$[9] and pale-green rods of $\mathbf{7}(Sb_2F_{11})_2$ (5% by weight) imbedded in the solid matrix of $\mathbf{10}(Sb_2F_{11})_2$ was carried out as previously described.[4f] The mixture of $S_4(AsF_6)_2$ and $S_8(AsF_6)_2$ (1:1 ratio) was prepared by condensing AsF_5 and traces of Br_2 onto S_8 (vacuum-dried) in the appropriate mole ratio in liquid SO_2[22] and $S_4(AsF_6)_2$ as previously described.[23] S_8 flowers (Anachemia) were vacuum-dried prior to use. SO_2 (Liquid Air), AsF_3 (Ozark-Mahoning), SO_2ClF (Aldrich), and Br_2 (Fisher) were stored over CaH_2, NaF, a mixture of 3 and 5 Å molecular sieves, and P_4O_{10}, respectively. AsF_5 was prepared according to reference 24. $(CN)_2$ (Matheson) was used as received, and SbF_5 (Ozark-Mahoning) was distilled in vacuo prior to use.

2.2. General Procedures. All reactions were performed in two-bulb, two-valve Pyrex vessels incorporating 25 mL bulbs and a medium sintered-glass frit using techniques that have been previously described.[25] Solid reagents and crystals were manipulated and handled under a nitrogen atmosphere in a drybox. FT-IR spectra of Nujol mulls between KBr disks were recorded at 293 K on a Bruker IFS66 FT-IR spectrometer at a resolution of 2.0 cm^{-1}. FT-Raman spectra were recorded at 120 K on a Bruker IFS66 FT-IR spectrometer equipped with a Bruker FRA106 FT-Raman accessory using a Nd:YAG laser (emission wavelength = 1064 nm; maximum laser power = 300 mW) in 5 mm Pyrex NMR tubes. Data were collected in the backscattering mode (180° excitation; resolution 2.0 cm^{-1}). A UV/vis spectrum of $\mathbf{7}(AsF_6)_2$ in a SO_2/AsF_5 solution was obtained on a Perkin-Elmer UV/vis spectrometer in a quartz cell of 1 mm path length attached to a glass vessel fitted with a Rotoflo valve. Elemental analyses of $\mathbf{7}(AsF_6)_2$, $\mathbf{7}(Sb_2F_{11})_2$, and $\mathbf{7}(SbF_6)_2$ were obtained from Mikroanalytisches Laboratorium Beller, Göttingen, Germany, and Galbraith Laboratories, Inc., Knoxville, TN.

2.3. Syntheses. 2.3.1. Preparation of $\mathbf{7}(AsF_6)_2$ from $(CN)_2$ and a 1:1 Mixture of $S_8(AsF_6)_2$ and $S_4(AsF_6)_2$. ***Caution!*** *Manipulations with very poisonous cyanogen should be carried out in a good vacuum line and very efficient fume hood.* $(CN)_2$ (0.490 g, 9.42 mmol) was condensed at 77 K into one bulb of a two-bulb vessel and dissolved in ca. 10 mL of SO_2. The solution was poured into the second bulb containing a 1:1 mixture of $S_4(AsF_6)_2$ and $S_8(AsF_6)_2$, "S_3AsF_6" (3.78 g, 13.2 mmol), and the mixture was stirred for 3 h to produce a brown precipitate under a pale-green solution. The volatiles were removed to constant weight, leaving 5.08 g of a dark-brown solid (calcd: 4.96 g based

(13) (a) Veciana, J.; Rovira, C.; Crespo, M. I.; Armet, O.; Domingo, V. M.; Palacio, F. *J. Am. Chem. Soc.* **1991**, *113*, 2552. (b) Veciana, J.; Rovira, C.; Ventosa, N.; Crespo, M. I.; Palacio, F. *J. Am. Chem. Soc.* **1993**, *115*, 57. (c) Ballester, M.; Pacual, I.; Carreras, C.; Vidal-Gancedo, J. *J. Am. Chem. Soc.* **1994**, *116*, 4205. (d) Viadel, L. I.; Carilla, J.; Labarta, A.; Juliá, L. *J. Mater. Chem.* **1998**, *8*, 1165. (e) Sedó, J.; Ventosa, N.; Ruiz-Molina, D.; Mas, M.; Molins, E.; Rovira, C.; Veciana, J. *Angew. Chem., Int. Ed.* **1998**, *37*, 330.

(14) (a) Bock, H.; John, A.; Havlas, Z.; Bats, J. W. *Angew. Chem., Int. Ed. Engl.* **1993**, *32*, 416. (b) Allinson, G.; Bushby, R. J.; Paillaud, J.-P. *J. Am. Chem. Soc.* **1993**, *115*, 2062. (c) Stickley, K. R.; Blackstock, S. C. *J. Am. Chem. Soc.* **1994**, *116*, 11576. (d) Michinobu, T.; Takahashi, M.; Tsuchida, E.; Nishide, H. *Chem. Mater.* **1999**, *11*, 1969. (e) Murata, H.; Takahashi, M.; Namba, K.; Takahashi, N.; Nishide, H. *J. Org. Chem.* **2004**, *69*, 631.

(15) For main-group diradicals, see: (a) Grützmacher, H.; Breher, F. *Angew. Chem., Int. Ed.* **2002**, *41*, 4006. (b) Power, P. P. *Chem. Rev.* **2003**, *103*, 789. (c) Breher, F. *Coord. Chem. Rev.* **2007**, *251*, 1007. (d) Hicks, R. G. *Org. Biomol. Chem.* **2007**, *5*, 1321.

(16) (a) Rajca, A. *Chem. Rev.* **1994**, *94*, 871. (b) Matasuda, K.; Iwamura, H. *Curr. Top. Solid State Mater. Sci.* **1997**, *2*, 446.

(17) (a) Salem, L.; Rowland, C. *Angew. Chem., Int. Ed. Engl.* **1972**, *11*, 92. (b) Borden, W. T. Diradicals. In *Encyclopedia of Computational Chemistry*; Schleyer, P. v. R. , Ed.; Wiley-Interscience: New York, 1998; p 708.

(18) (a) Recently, examples of main-group diradicals that are paramagnetic in the solid state have been reported, but as far as we are aware, they either contain spacer groups between the radical centers, are stabilized bulky groups, or are much more complicated than the systems in the subclass. For examples, see: (b) Konarev, D. V.; Khasanov, S. S.; Otsuka, A.; Saito, G.; Lyubovskaya, R. M. *J. Am. Chem. Soc.* **2006**, *128*, 9292. (c) Gilroy, J. B.; McKinnon, S. D. J.; Kennepohl, P.; Zsombor, M. S.; Ferguson, M. J.; Thompson, L. K.; Hicks, R. G. *J. Org. Chem.* **2007**, *72*, 8062. (d) Rajca, A.; Takahashi, M.; Pink, M.; Spagnol, G.; Rajca, S. *J. Am. Chem. Soc.* **2007**, *129*, 10159. (e) Rajca, A.; Shiraishi, K.; Rajca, S. *Chem. Commun.* **2009**, 4372.

(19) Genin, H.; Hoffmann, R. *Macromolecules* **1998**, *31*, 444.

(20) Wood, D. Ph.D. Thesis, University of New Brunswick, Fredericton, Canada, 2001.

(21) Scherer, W.; et al. Unpublished results.

(22) Gillespie, R. J.; Passmore, J.; Ummat, P. K.; Vaidya, O. *Inorg. Chem.* **1971**, *10*, 1327.

(23) Murchie, M. P.; Passmore, J.; Sutherland, G. W.; Kapoor, R. *J. Chem. Soc., Dalton Trans.* **1992**, 503.

(24) Aris, D. R.; Knapp, C.; Passmore, J.; Wang, X. *J. Fluorine Chem.* **2005**, *126*, 1368.

(25) (a) Murchie, M.; Passmore, J. *Inorg. Synth.* **1986**, *24*, 76. (b) Murchie, M. P.; Kapoor, R.; Passmore, J.; Schatte, G.; Way, T. *Inorg. Synth.* **1997**, *31*, 102.

Scheme 1

$$S_4(AsF_6)_2 + S_8(AsF_6)_2 + 2\ (CN)_2 \rightarrow 2\ \mathbf{7}(AsF_6)_2 \quad (2)$$

$$13\ S_4(AsF_6)_2 + 8\ (CN)_2 + 4\ SO_2 \rightarrow\ 8\ \mathbf{7}(AsF_6)_2 + 8\ OSF_2 + 7\ AsF_5 + 3\ AsF_3 \quad (3)$$

$$S_{10}(AsF_6)_2 + (CN)_2 \rightarrow \mathbf{7}(AsF_6)_2 + \tfrac{1}{2}\ S_8 \quad (4)$$

$$S_{16}(AsF_6)_2 + (CN)_2 \rightarrow \mathbf{7}(AsF_6)_2 + {}^{5}/_{4}\ S_8 \quad (5)$$

$$3\ S_8 + 16\ SbF_5 \rightarrow 2\ S_4(SbF_6)_2 + 2\ S_8(SbF_6)_2 + 4\ SbF_3{\bullet}SbF_5 \quad (6)$$

$$S_4(SbF_6)_2 + S_8(SbF_6)_2 + 2\ (CN)_2 \rightarrow 2\ \mathbf{7}(SbF_6)_2 \quad (7)$$

$$\mathbf{7}(AsF_6)_2 + 4\ SbF_5 \rightarrow \mathbf{7}(Sb_2F_{11})_2 + 2\ AsF_5 \quad (8)$$

$$\mathbf{10}(AsF_6)_2 + 4\ SbF_{5(exc.)} \rightarrow \mathbf{10}(Sb_2F_{11})_2 + 2\ AsF_5 \quad (9)$$

$$\mathbf{7}(AsF_6)_2 + Na_2S_2O_4 \rightarrow \mathbf{7}(AsF_6) + 2\ NaAsF_6 + 2\ SO_2 \rightarrow \ldots \quad (10)$$

on eq 2 in Scheme 1). Suitable single crystals of $\mathbf{7}(AsF_6)_2$ were obtained as dark-red-brown plates from a AsF_3 solution by the slow removal of the solvent at 5 °C over several days into a collection bulb held at 0 °C. Elem anal. Obsd/calcd for $C_2N_2S_6As_2F_{12}$: C, 3.87/3.86; N, 4.48/4.52; S, 30.98/30.91; As, 23.92/24.08; F, 36.20/36.63. UV/vis (SO_2/AsF_5) λ_{max}/nm (log ε/M^{-1} cm^{-1}): 338 (2.5), 430 (1.4), 600 (0.4), 644 (0.5), 704 (0.3). The actual UV/vis spectrum is shown in Figure S1 in the Supporting Information.

2.3.2. Preparation of $\mathbf{7}(AsF_6)_2$ from $(CN)_2$ and $S_4(AsF_6)_2$. $(CN)_2$ (0.345 g, 6.63 mmol) was condensed onto $S_4(AsF_6)_2$ (3.42 g, 6.77 mmol) at 77 K in ca. 8 mL of SO_2. The mixture was warmed up to room temperature and stirred for 1 h to produce a pale-green solution over a dark-brown crystalline solid. Removal of the volatiles left 2.56 g of reddish-brown crystalline solid (calcd: 2.59 g based on eq 3 in Scheme 1). The FT-Raman spectrum of the product was identical with that of $\mathbf{7}(AsF_6)_2$, prepared as described in section 2.3.1. Elem anal. Obsd/calcd for $C_2N_2S_6As_2F_{12}$: C, 3.98/3.86; N, 4.63/4.52; S, 31.00/30.91; As, 24.22/24.08; F, 36.17/36.63.

2.3.3. Preparation of $\mathbf{7}(SbF_6)_2$. SO_2 (16.5 g), SbF_5 (7.55 g, 34.8 mmol), and Br_2 (~15 mg) were condensed onto S_8 (1.52 g, 5.93 mmol) to give a dark-blue solution over a colorless precipitate after 1 day. The dark-blue solution was filtered and the precipitate washed several times with small portions of SO_2. The FT-Raman spectrum of the colorless solid (2.34 g) was consistent with the presence of $(SbF_3)_3SbF_5$[26] and/or $(SbF_3)_6(SbF_5)_5$,[27] as well as some other unidentified material. $(CN)_2$ (0.615 g, 11.8 mmol) was condensed onto the filtered blue solution at 77 K to produce, upon warming to room temperature, a dark-green solution over a reddish-brown precipitate. The mixture was stirred for 3 days, and the volatiles were removed under a dynamic vacuum, leaving 7.28 g of an inhomogeneous mixture of reddish-brown shiny crystals (clean, no coated faces), reddish-brown crystals coated by other solids, an amorphous-like brown solid, and a small quantity of white solid (observed as small specks throughout the brown solid). The X-ray crystal structure of $\mathbf{7}(SbF_6)_2$ was determined using the well-shaped shiny crystals. Variable-temperature magnetic, IR, and Raman measurements were obtained on what appeared to be clean crystals separated manually in the drybox. The X-ray structure reported below was obtained from a crystal stored for several years.

2.3.4. Preparation of $\mathbf{7}(Sb_2F_{11})_2$. SO_2 (11.8 g) and SbF_5 (9.69 g, 44.7 mmol) were condensed at 77 K onto $\mathbf{7}(AsF_6)_2$ (1.70 g, 2.72 mmol), giving a dark-green solution upon warming to room temperature. The mixture was stirred for 3 days, and the volatiles were removed under a dynamic vacuum to constant weight, leaving 3.13 g of a dark-green solid (calcd: 3.14 g of $\mathbf{7}(Sb_2F_{11})_2$ based on eq 8 in Scheme 1). The crystals of $\mathbf{7}(Sb_2F_{11})_2$ were grown from an SO_2/SO_2ClF mixture (2:1 mole ratio) by slow evaporation of the solvent at room temperature, while the collection bulb was held at 0 °C. Dark-green crystalline rods and some reddish-brown platelike crystals, visible under a microscope, were obtained. Crystallization at a lower temperature seemed to increase the fraction of the red-brown phase. The identity of both phases was confirmed by their X-ray structures.[20] The X-ray structure reported below was obtained on a red crystal stored for several years. It was red in transmitted light but seemed green in reflected light. Some crystals were coated in a green powder, which was removed when the crystals were scratched. Elem anal. Obsd/calcd for $C_2N_2S_6Sb_4F_{22}$: C, 2.04/2.09; N, 2.46/2.44; S, 15.60/16.74; Sb, 42.00/42.37; F, 37.90/36.37.

2.3.5. Preparation of $(CNSNS)_2(Sb_2F_{11})_2$ [$\mathbf{10}(Sb_2F_{11})_2$]. SO_2 (18.3 g) and SbF_5 (20.1 g, 92.7 mmol) were condensed onto $\mathbf{10}(AsF_6)_2$ (1.50 g, 2.56 mmol) at 77 K, giving a pale-yellow solution upon warming to room temperature. The mixture was stirred for 3 days, and the volatiles were removed under a dynamic vacuum to constant weight, leaving 2.86 g of a very pale-yellow crystalline solid (calcd: 2.85 g based on eq 9 in Scheme 1). $\mathbf{10}(Sb_2F_{11})_2$ was a pale-yellow solid that was indefinitely stable under dry nitrogen at room temperature. The structure of $\mathbf{10}(Sb_2F_{11})_2$ was confirmed by X-ray diffraction, which showed the dication $\mathbf{10}^{2+}$ to be structurally identical with that in $\mathbf{10}(AsF_6)_2$ reported previously.[9] FT-Raman spectrum (cm^{-1}): [dication peaks][9] 1499s, 1300vw, 1205w, 954 mw, 795s, 591 m, 540vw, 473s, 441mw, 292mw, 282mw, 219vs, 189vw, 154vs; [$Sb_2F_{11}^-$ anion peaks] 684w, 646 m, 559vw, 354w.

2.3.6. Preparation of $\mathbf{7}(Sb_2F_{11})_2$ Imbedded in a Matrix of Isomorphous $\mathbf{10}(Sb_2F_{11})_2$. SO_2 (10.8 g) was condensed at 77 K onto a mixture of $\mathbf{10}(Sb_2F_{11})_2$ (0.893 g, 0.802 mmol) and $\mathbf{7}(Sb_2F_{11})_2$ (0.392 g, 0.341 mmol) to form a dark-green solution upon warming to room temperature. The crystalline sample (large pale-green rectangular rods) was prepared by slow evaporation of the solvent with a temperature gradient of 5 °C (collection bulb, 0 °C; bulb containing the mixture, 5 °C) for 6 h. The crystals were isolated by filtration. One of the crystals was examined by X-ray and found to have the same unit cell parameters as those in $\mathbf{10}(Sb_2F_{11})_2$. These crystals were used to obtain variable-temperature magnetic susceptibility measurements of $\mathbf{7}$-$(Sb_2F_{11})_2$ diluted in a diamagnetic matrix of $\mathbf{10}(Sb_2F_{11})_2$, as described in section 2.7. The slow removal of SO_2 from the supernatant solution produced smaller and darker-green rods, which were not used for magnetic studies.

2.3.7. Reduction of $\mathbf{7}(AsF_6)_2$. SO_2 (10.6 g) was condensed at 77 K onto a mixture of $\mathbf{7}(AsF_6)_2$ (1.30 g, 2.08 mmol) and $Na_2S_2O_4$ (0.189 g, 1.09 mmol) into a vessel equipped with an EPR tube to produce a yellow-brown solution over a black solid upon warming to room temperature. A portion of the soluble fraction was poured into an attached EPR tube, and an EPR spectrum was obtained at 193 K (Figure S6 in the Supporting Information). After 24 h, yellow crystals of S_8 (FT-Raman) had precipitated and continued to precipitate until the volatiles were removed to constant weight, leaving after 3 days 1.39 g of an inhomogeneous mixture of pale-yellow crystals of S_8 (FT-Raman), colorless crystals of $NaAsF_6$ (X-ray), and a black solid. The sulfur was extracted from the mixture using CS_2 (10.5 g), leaving 1.25 g of $NaAsF_6$ and the black solid (expected total mass of $NaAsF_6$ and proposed $\mathbf{7}AsF_6$ is 1.34 g assuming a quantitative reaction according to Scheme 1, eq 10). A small amount of black solid was manually separated from the crystals of $NaAsF_6$, and the FT-Raman spectrum of the black solid was obtained (Figure S5 in the Supporting Information). Attempts to grow crystals of this material from SO_2 were unsuccessful. When a small amount of black solid was redissolved in SO_2, precipitation of sulfur crystals was observed after 10 min. The soluble fraction was filtered and evaporated, producing the

(26) Nandana, W. A. S.; Passmore, J.; Swindells, D. C. N; Taylor, P.; White, P. S.; Vekris, J. E. *J. Chem. Soc., Dalton Trans.* **1983**, 619.
(27) Nandana, W. A. S.; Passmore, J.; White, P. S. *J. Chem. Soc., Dalton Trans.* **1985**, 1623.

Chart 2

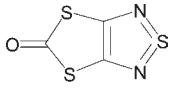

18

black solid with no change in the FT-Raman spectrum. Upon heating of this black solid at 100 °C, a small amount of **18**[28] (Chart 2) sublimed out (X-ray). The FT-Raman spectrum of the black residue was the same as that prior to heating.

2.4. Chemical Stability, Solubility, and Some Physical Properties of the Salts of 7^{2+}. All of the salts of 7^{2+} are indefinitely stable under dry nitrogen at room temperature, but exposure to moisture gives a white mist and a yellow solid (S_8, FT-Raman). Upon heating $7(MF_6)_2$ to 200 °C, sulfur is sublimed out. Heating of $7(Sb_2F_{11})_2$ resulted in evolution of a white mist, which condensed as colorless droplets (assumed to be SbF_5). $7(MF_6)_2$ is sparingly soluble in SO_2 (M = As, 0.012 g mL^{-1}; M = Sb, 0.027 g mL^{-1}), while the solubility of $7(Sb_2F_{11})_2$ in SO_2 is greater (0.057 g mL^{-1}). All three salts are very soluble in the SO_2/AsF_5 mixture and pure AsF_3. All solutions are green. When smeared against a hard surface or ground using a mortar and pestle, $7(MF_6)_2$ (M = As, Sb) changes color from red-brown to green. The magnetic moment of $7(AsF_6)_2$ increased from 2.62 to 3.33 μ_B (determined by the Gouy method) for a sample ground for 1 h.

2.5. Crystal Structure Determinations. The measurements were made on a Rigaku RAXIS diffractometer [$7(SbF_6)_2$ and $7(Sb_2F_{11})_2$] and an Enraf Nonius CAD-4 diffractometer [**10**-$(Sb_2F_{11})_2$]. The structures were solved by direct methods, and all of the atoms were refined anisotropically.[29] Data collection and refinement parameters are listed in Table 1, except for $7(AsF_6)_2$ [isomorphous to $7(SbF_6)_2$], which was given in a preliminary communication.[4a] Figures illustrating the crystal structures were prepared using *DIAMOND*,[30] which was also used to determine all of the quoted *inter*molecular parameters.

2.6. EPR Spectroscopy. All of the EPR spectra were obtained using a modified Varian spectrometer. Samples for solution EPR studies were prepared in a two-bulb vessel equipped with a 4 mm quartz tube. The following amounts were used: $7(AsF_6)_2$, 0.161 g (0.259 mmol) in a SO_2/AsF_5 mixture (8.196/0.980 g); $7(SbF_6)_2$, 0.251 g (0.351 mmol) in a SO_2/AsF_5 mixture (12.144/1.437 g); $7(Sb_2F_{11})_2$, 0.049 g (0.042 mmol) in a SO_2/SbF_5 mixture (5.328/1.624 g). All solutions were dark green in color and contained no insoluble material. Isotropic EPR spectra were recorded at +20 and −80 °C; anisotropic frozen solution spectra were recorded at −160 °C. Single-crystal EPR studies of **7**-$(Sb_2F_{11})_2$ doped in a diamagnetic host have been described elsewhere.[4f]

2.7. Magnetic Susceptibility Measurements. The variable-temperature magnetic susceptibilities of red-brown $7(AsF_6)_2$, red-brown $7(SbF_6)_2$, and light-green $7(Sb_2F_{11})_2$ doped in diamagnetic $\mathbf{10}(Sb_2F_{11})_2$ were determined using a Quantum Design (MPMS) SQUID magnetometer operating at a field of 1 T. The actual numerical data are given in Table S1 in the Supporting Information. The experimental magnetic data of $7(Sb_2F_{11})_2$ diluted in a diamagnetic host were fitted by the Bleaney−Bowers model,[31] and those of $7(MF_6)_2$ (M = As, Sb) were fitted by both the Hall model[32] for one-dimensional (1D) chains and the Lines model[33] for two-dimensional (2D) sheets.

2.8. Quantum-Chemical Calculations. The results for single-reference density functional theory (DFT) calculations were obtained using the *Gaussian 03* suite of programs.[34] The commonly used Pople split-valence double-ζ basis set, 6-31G*, was employed in single-reference calculations. For DFT calculations, a hybrid functional by Perdew, Burke, and Ernzerhof (PBE0),[35] which has no thermodynamically fitted parameters, was chosen. The geometry of 7^{2+} was constrained to C_{2h} symmetry in all cases, except when a relaxed potential energy scan about the C−C bond was performed. The effects of other DFT functionals (B3LYP and MPW1PW91) as well as inclusion of extra polarization and diffuse functions and expansion of the valence basis set to triple-ζ quality were tested and found to give nearly identical results (Table S2 in the Supporting Information). DFT calculations predicted a triplet ground state for 7^{2+}. The "closed-shell" singlet state was found to be significantly higher in energy than the triplet state. Because of the significantly larger energy separation between the "closed-shell" singlet and triplet states compared to the experimental singlet−triplet gap, symmetry-broken UPBE0 calculations were performed to find a ("open-shell") singlet diradical state.

The use of symmetry-broken methods provides only a qualitative description of the singlet diradical state. The proper treatment of a static electron correlation in singlet diradical states requires the use of multiconfigurational methods.[36] The Molpro program[37] was employed for multiconfiguration calculations on the lowest singlet and triplet states of 7^{2+}. Geometry optimizations of 7^{2+} were done using CASSCF[38] with two different active spaces and Pople's split-valence triple-ζ 6-311G* basis set. The smaller active space consisted of eight electrons distributed to the four highest occupied and lowest unoccupied orbitals of the reference Hartree-Fock wave function constituting an [8, 8] active space. The larger active space was augmented to include two more occupied and unoccupied orbitals, leading to a [12, 12] active space. The dynamical electron correlation to the

(28) Underhill, A. E.; Hawkins, I.; Edge, S.; Wilkes, S. B.; Varma, K. S.; Kobayashi, A.; Kobayashi, H. *Synth. Met.* **1993**, *55*−*57*, 1914.
(29) Sheldrick, G. M. *SHELX-97, Program for the Refinement of Crystal Structures*; University of Göttingen: Göttingen, Germany, 1997.
(30) *DIAMOND*, version 3.2d; Crystal Impact: Bonn, Germany, 1997−2010.
(31) Bleany, B.; Bowers, K. D. *Proc. R. Soc. London, Ser. A* **1952**, *214*, 451.
(32) (a) Estes, W. E.; Hatfield, W. E.; Van Ooijen, J. A. C.; Reedijk, J. *J. Chem. Soc., Dalton Trans.* **1980**, 2121. (b) Hall, J. W. Ph.D. Thesis, University of North Carolina, Raleigh, NC, 1977.
(33) Lines, M. E. *J. Phys. Chem. Solids* **1970**, *31*, 101.
(34) Frisch, M. J.; Trucks, G. W.; Schlegel, H. B.; Scuseria, G. E.; Robb, M. A.; Cheeseman, J. R.; Montgomery, J. A., Jr.; Vreven, T.; Kudin, K. N.; Burant, J. C.; Millam, J. M.; Iyengar, S. S.; Tomasi, J.; Barone, V.; Mennucci, B.; Cossi, M.; Scalmani, G.; Rega, N.; Petersson, G. A.; Nakatsuji, H.; Hada, M.; Ehara, M.; Toyota, K.; Fukuda, R.; Hasegawa, J.; Ishida, M.; Nakajima, T.; Honda, Y.; Kitao, O.; Nakai, H.; Klene, M.; Li, X.; Knox, J. E.; Hratchian, H. P.; Cross, J. B.; Bakken, V.; Adamo, C.; Jaramillo, J.; Gomperts, R.; Stratmann, R. E.; Yazyev, O.; Austin, A. J.; Cammi, R.; Pomelli, C.; Ochterski, J. W.; Ayala, P. Y.; Morokuma, K.; Voth, G. A.; Salvador, P.; Dannenberg, J. J.; Zakrzewski, V. G.; Dapprich, S.; Daniels, A. D.; Strain, M. C.; Farkas, O.; Malick, D. K.; Rabuck, A. D.; Raghavachari, K.; Foresman, J. B.; Ortiz, J. V.; Cui, Q.; Baboul, A. G.; Clifford, S.; Cioslowski, J.; Stefanov, B. B.; Liu, G.; Liashenko, A.; Piskorz, P.; Komaromi, I.; Martin, R. L.; Fox, D. J.; Keith, T.; Al-Laham, M. A.; Peng, C. Y.; Nanayakkara, A.; Challacombe, M.; Gill, P. M. W.; Johnson, B.; Chen, W.; Wong, M. W.; Gonzalez, C.; Pople, J. A. *Gaussian 03*, revision C.02; Gaussian, Inc.: Wallingford, CT, 2004.
(35) (a) Perdew, J. P.; Ernzerhof, M.; Burke, K. *J. Chem. Phys.* **1996**, *105*, 9982. (b) Perdew, J. P.; Burke, K.; Ernzerhof, M. *Phys. Rev. Lett.* **1996**, *77*, 3865–3868. *Phys. Rev. Lett.* **1997**, *78*, 1396.
(36) Bally, T.; Borden, W. T. Calculations on Open-Shell Molecules: A Beginner's Guide. In *Reviews in Computational Chemistry*; Lipkowitz, K. B., Boyd, D. B., Eds.; Wiley-VCH: New York, 1999; Vol. *13*, pp 1−97.
(37) Werner, H.-J.; Knowles, P. J.; Lindh, R.; Manby, F. R.; Schütz, M.; Celani, P.; Korona, T.; Mitrushenkov, A.; Rauhut, G.; Adler, T. B.; Amos, R. D.; Bernhardsson, A.; Berning, A.; Cooper, D. L.; Deegan, M. J. O.; Dobbyn, A. J.; Eckert, F.; Goll, E.; Hampel, C.; Hetzer, G.; Hrenar, T.; Knizia, G.; Köppl, C.; Liu, Y.; Lloyd, A. W.; Mata, R. A.; May, A. J.; McNicholas, S. J.; Meyer, W.; Mura, M. E.; Nicklass, A.; Palmieri, P.; Pflüger, K.; Pitzer, R.; Reiher, M.; Schumann, U.; Stoll, H.; Stone, A. J.; Tarroni, R.; Thorsteinsson, T.; Wang, M.; Wolf, A. *MOLPRO, a package of ab initio programs*, version 2006.1; see http://www.molpro.net.
(38) (a) Werner, H.-J.; Knowles, P. J. *J. Chem. Phys.* **1985**, *82*, 5053. (b) Knowles, P. J.; Werner, H.-J. *Chem. Phys. Lett.* **1985**, *115*, 259. (c) Busch, T.; Degli Esposti, A.; Werner, H.-J. *J. Chem. Phys.* **1991**, *94*, 6708.

Table 1. Crystal Data and Structure Refinement Details for $\mathbf{7}(SbF_6)_2$, $\mathbf{7}(Sb_2F_{11})_2$, and $\mathbf{10}(Sb_2F_{11})_2$

	$\mathbf{7}(SbF_6)_2$	$\mathbf{7}(Sb_2F_{11})_2$	$\mathbf{7}(Sb_2F_{11})_2$	$\mathbf{10}(Sb_2F_{11})_2$[a]
empirical formula	$CNSSbF_6$	$CNSSb_2F_{11}$	$C_2N_2S_6Sb_4F_{22}$	$C_2N_2S_6Sb_4F_{22}$
fw	357.9	574.68	1149.36	1113.3
temperature (K)	173	296	123	293
λ (Å)	0.710 73	0.710 70	0.710 73	0.710 73
space group	$P\bar{1}$	$P\bar{1}$	$P\bar{1}$	$P\bar{1}$
cryst syst	triclinic	triclinic	triclinic	triclinic
color and habit	dark red, block	dark red, block	dark red, block	pale yellow, parallelepipeds
a (Å)	5.6403(12)	8.4380(14)	8.4307(11)	8.171(3)
b (Å)	7.9108(18)	8.9554(12)	8.7468(11)	8.616(2)
c (Å)	9.2776(16)	10.5349(8)	10.2677(11)	10.333(3)
α (deg)	98.550(9)	103.31(3)	100.978(3)	102.30(2)
β (deg)	92.427(7)	101.40(3)	101.941(1)	101.50(3)
γ (deg)	103.476(12)	118.68(3)	118.442(3)	117.76(2)
volume (Å ^{3})	396.81(14)	633.84(36)	613.5(2)	590.3(3)
Z	2	2	1	1
density (g cm^{-3})	2.996	3.011	3.111	3.132
μ (mm^{-1})	4.307	4.863	5.025	5.056
reflns collected	13 447	28 552	13 806	3865
indep reflns	1614	5455	2654	3341
R1[b], wR2[c]	0.0681, 0.2156	0.0376, 0.0480	0.0346, 0.0418	0.0392, 0.0957

[a] From ref 20. [b] $R1 = \sum||F_o| - |F_c||/\sum|F_o|$. [c] $wR2 = \{\sum[w(F_o^2 - F_c^2)^2]/\sum[F_o^4]\}^{1/2}$.

CASSCF state energies was included in a perturbational manner using the CASPT2 method.[39]

[12,12]-CASSCF-optimized geometries of the triplet and singlet electronic states of $\mathbf{7}^{2+}$ and PBE0-optimized geometries of the triplet and closed-shell singlet states are included in Table 4. The harmonic vibrational frequencies of the PBE0-optimized triplet and open-shell singlet states of $\mathbf{7}^{2+}$ are listed in Table 5. The vibrational modes were assigned by normal-coordinate analysis and visualization of the calculated frequencies. For the normal-coordinate analysis, Cartesian force constants calculated for a PBE0/TZVPP-optimized structure[35,40] were transformed into more descriptive internal coordinates using the *Turbomole* program.[41] Descriptions of the internal coordinates and assignment of calculated normal modes to internal coordinates have been presented in Tables S3 and S4 in the Supporting Information. The rotational profile about the C−C bond was examined by performing a UPBE0 relaxed potential energy scan by varying the N−C−C−N dihedral angle from 0 to 180°. The effect of solvent SO_2 on the rotational profile was examined by repeating the scan using the IEFPCM solvent model.[42] Dielectric constant 14.0 and solvent radius 2.032 Å were applied for the SO_2 solvent.

3. Results and Discussion

3.1. Syntheses of $(CNSSS)_2(A)_2$ (A = AsF_6^-, SbF_6^-, $Sb_2F_{11}^-$) and $\mathbf{10}(Sb_2F_{11})_2$. The reaction of an excess of $(CN)_2$ and a 1:1 mixture of $S_4(AsF_6)_2$ and $S_8(AsF_6)_2$ proceeded to produce the reddish-brown pure $\mathbf{7}(AsF_6)_2$ (IR, Raman, and elemental analysis) in an almost quantitative yield (Scheme 1, eq 2).

The same reddish-brown solid was obtained from the reaction between $(CN)_2$ and $S_4(AsF_6)_2$ (Scheme 1, eq 3). Both products have been shown to be identical by elemental analysis and vibrational spectroscopy. $\mathbf{7}(AsF_6)_2$ can also be obtained by the reactions of $(CN)_2$ and "$S_{10}(AsF_6)_2$" and "$S_{16}(AsF_6)_2$" (Scheme 1, eqs 4 and 5, respectively).[20] The FT-Raman spectra of the products from the latter two reactions show peaks attributable to $\mathbf{7}(AsF_6)_2$ and sulfur, but the observed weight changes and the in situ EPR spectra of these reactions (see section 3.6) indicate also the presence of other species.

The synthesis of $\mathbf{7}(SbF_6)_2$ (Scheme 1, eq 7) was carried out similarly to $\mathbf{7}(AsF_6)_2$ but using SbF_5 instead of AsF_5 (Scheme 1, eq 6). We note that $S_4(SbF_6)_2$ and $S_8(SbF_6)_2$ have not yet been isolated in the solid state, and we do not suggest that these species are actually formed. The product obtained from reaction (7) appears as an inhomogeneous mixture of highly crystalline red $\mathbf{7}(SbF_6)_2$ (X-ray crystal structure) and small amounts of a colorless solid (reduced antimony fluorides).[26,27] The clean red crystals were manually separated from the product mixture under the microscope, and the FT-Raman spectrum (Figure S2 in the Supporting Information) obtained on these crystals showed two peaks at 654 and 651 cm^{-1}, which could not be assigned to either the dication or the SbF_6^- anion but which matched very well with the most intense peak (653 cm^{-1}) observed in the FT-Raman spectrum of the reduced antimony fluorides isolated from reaction (6).

The preparation of $\mathbf{7}(Sb_2F_{11})_2$ was carried out by reacting pure $\mathbf{7}(AsF_6)_2$ with a large molar excess of SbF_5 (Scheme 1, eq 8). After removal of the excess SbF_5 in a vacuum, pure $\mathbf{7}(Sb_2F_{11})_2$ (IR, Raman, elemental analysis) was obtained in an almost quantitative yield. This salt was used for cocrystallization with $\mathbf{10}(Sb_2F_{11})_2$ (prepared analogously, Scheme 1, eq 9) to obtain the sample of $\mathbf{7}^{2+}$ "diluted" in a diamagnetic host studied by magnetic susceptibility measurements.

3.2. Reduction of $\mathbf{7}^{2+}$. Evidence for the Radical Cation $\mathbf{7}^+$. Reduction experiments of $\mathbf{7}(AsF_6)_2$ (Scheme 1, eq 10) were performed to prepare the monoradical monocation $\mathbf{7}^{\bullet+}$, which potentially could form a structure with stronger interactions between the heterocyclic rings, leading to interesting

(39) (a) Werner, H.-J. *Mol. Phys.* **1996**, *89*, 645. (b) Celani, P.; Werner, H.-J. *J. Chem. Phys.* **2000**, *112*, 5546.
(40) (a) Weigend, F.; Ahlrichs, R. *Phys. Chem. Chem. Phys.* **2005**, *7*, 3297. (b) Metz, B.; Stoll, H.; Dolg, M. *J. Chem. Phys.* **2000**, *113*, 2563.
(41) (a) *TURBOMOLE, Program Package for ab initio Electronic Structure Calculations*, version 5.10; TURBOMOLE GmbH: Karlsruhe, Germany, 2008. (b) Ahlrichs, R.; Bär, M.; Häser, M.; Horn, H.; Kölmel, C. *Chem. Phys. Lett.* **1989**, *162*, 165.
(42) (a) Cancès, E.; Mennucci, B.; Tomasi, J. *J. Chem. Phys.* **1997**, *107*, 3032. (b) Cossi, M.; Barone, V.; Mennucci, B.; Tomasi, J. *Chem. Phys. Lett.* **1998**, *286*, 253.

bulk properties. Herein we present some spectroscopic evidence for the formation of a solid containing $\mathbf{7}(AsF_6)$, but the X-ray structure could not be obtained.

Reaction (10) (Scheme 1) proceeded to form an inhomogeneous mixture of S_8, $NaAsF_6$, and a black solid proposed to be $\mathbf{7}(AsF_6)$. Notably, the FT-Raman and IR spectra (see Figure S5 in the Supporting Information and ref 20) of this product were similar to that of $\mathbf{7}(AsF_6)_2$, except that the majority of the peaks were shifted to significantly lower wavenumbers (e.g., the C=N stretch at 1513 cm^{-1} in $\mathbf{7}(AsF_6)_2$ and 1417 cm^{-1} in the black solid and the S−N stretch at 911 and 876 cm^{-1}, respectively). This observation is consistent with the weakening of the bonds within the rings arising from the addition of an electron to the π^* singly occupied molecular orbital (SOMO) of $\mathbf{7}^{2+}$ (see Figure 5). The C−C stretching frequencies (1192 cm^{-1} in $\mathbf{7}(AsF_6)_2$ and 1190 cm^{-1} in the black solid) remained essentially unchanged, consistent with the nodal properties of SOMOs at the two C atoms.

The reduction of $\mathbf{7}^{2+}$ with $Na_2S_2O_4$ was monitored in situ by EPR. The recorded spectra showed two resonances: a singlet with $g = 2.0155$, attributed to the starting $\mathbf{7}^{2+}$, and a pentet with $g = 2.0132$ and a coupling constant $a_N = 2.0$ G (Figure S6 in the Supporting Information). The pentet almost certainly arises from the coupling of an unpaired electron to two equivalent N atoms, which could be the case for $\mathbf{7}^{\bullet+}$, assuming that the unpaired electron is delocalized over both rings. Examination of the molecular structure of $\mathbf{7}^{\bullet+}$ in the gas phase optimized at the UPBE0/6-31G* level of theory (C_i symmetry, true minimum) shows two slightly nonplanar equivalent −CNSSS rings with nitrogen hyperfine coupling constants of 1.0 G (Figure S7 in the Supporting Information). The puckered nature of the two rings indicates that the stabilizing π delocalization is reduced by the addition of the eighth π electron, and thus $\mathbf{7}^{\bullet+}$ is expected to be considerably less stable that the perfectly planar dication. The putative $\mathbf{7}(AsF_6)$ redissolved in SO_2 appeared to gradually decompose, losing elemental sulfur with the subsequent formation of unidentified products. The only identified product was **18** (Chart 2), obtained upon sublimation of the black residue given by evaporation of a filtrate separated from the elemental sulfur.

3.3. Crystal Structures of $\mathbf{7}(SbF_6)_2$ and $\mathbf{7}(Sb_2F_{11})_2$. The structure of red $\mathbf{7}(SbF_6)_2$ is isomorphous to red $\mathbf{7}(AsF_6)_2$, which was reported in a preliminary communication.[4a] Therefore, the following discussion of the structural features (including packing motifs) of $\mathbf{7}(SbF_6)_2$ is also relevant for $\mathbf{7}(AsF_6)_2$.

The dication $\mathbf{7}^{2+}$ is shown in Figure 1. The internal structural parameters of *centro*symmetric $\mathbf{7}^{2+}$ (Table 2) are not statistically different in $\mathbf{7}(MF_6)_2$ (M = As, Sb) and $\mathbf{7}(Sb_2F_{11})_2$ and are similar to those of the other salts of $RCNSSS^{\bullet+}$ reported previously.[1−3] SbF_6^- has a distorted O_h symmetry (see Figure S8 in the Supporting Information). The symmetrically *cis*-fluorine-bridged [$\angle$(SbFSb) = 148.1(2)°] $Sb_2F_{11}^-$ structure is ordered at −150 °C (see Figure S9 in the Supporting Information) and is similar to that previously reported in $Ir_4(CO)_8(\mu\text{-}F)_2(Sb_2F_{11})_2$.[43] The increase in disorder with temperature is discussed in the Supporting Information.

(43) Hwang, I.-C.; Seppelt, K. *Inorg. Chem.* **2003**, *42*, 7116.

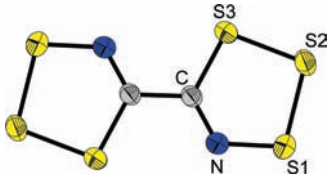

Figure 1. Depiction of $\mathbf{7}^{2+}$ [as visualized from the structure of $\mathbf{7}(SbF_6)_2$]. Thermal ellipsoids drawn at 50% probability.

The observed coordination numbers about each dication and anion in $\mathbf{7}(MF_6)_2$ (M = As, Sb) are 12 and 6, respectively. The analogous coordination numbers in $\mathbf{7}(Sb_2F_{11})_2$ are 10 and 5 (Figure S10 in the Supporting Information). We find that these observed arrangements fit the radius ratio rule for predicting coordination numbers based on the sizes of the cations and anions (see Table S7 in the Supporting Information).[44] Cation−anion contacts in the structures of $\mathbf{7}^{2+}$ (confined exclusively to S···F contacts)[45] were used to calculate the corresponding valency units by applying Brown's approach, which estimates an effective positive charge on each S atom in the dication assuming that the interaction is ionic.[46] The calculated values are listed in Table 3, where they are compared with the gas-phase natural bond orbital (NBO) atomic charges computed by a DFT method. The sum of the valency units for the three S atoms is close to unity, consistent with a charge of 1+ on each of the $-CNSSS^{\bullet+}$ rings, as is expected for an ionic structure.

The observed trans-planar geometry (C_{2h} symmetry) of $\mathbf{7}^{2+}$ is stabilized by *inter*-ring $S^{\delta+}\cdots N^{\delta-}$ electrostatic interactions (NBO charges listed in Table 3) and is the most stable of all of the other possible molecular arrangements (see computational analysis section 3.5). The dication consists of two 7π $CNSSS^{\bullet+}$ rings joined by a C−C single bond (1.462 Å, cf. 1.46 Å for a sp^2−sp^2 single bond distance).[47] The experimental geometrical parameters of $\mathbf{7}^{2+}$ are in good agreement with those predicted at the PBE0/6-31G* and [12,12]-CASSCF/6-311G* levels of theory (Table 4). The calculated geometries of both triplet and open-shell singlet states are almost identical, implying very weak or even negligible interaction between the unpaired electrons. The calculated atomic spin densities of the triplet state show that the spin density lies almost completely on the S atoms (Table 3) in a fashion similar to that of other trithiazolium radicals.[2,3] Thus, the two rings in the dication can be viewed as two independent monocations joined by a C−C single bond (albeit their electrons are very weakly interacting). This view is strongly

(44) Huheey, J. E.; Keiter, E. A.; Keiter, R. L. *Inorganic Chemistry: Principles of Structure and Reactivity*; 4th ed.; Harper Collins: New York, 1993.

(45) Contacts were only considered if their distances fell within the sum of the van der Waals radii of the atoms in question (C−F = 3.05 Å, N−F = 2.90 Å, and S−F = 3.50 Å). There were no C−F and N−F contacts found that were less than these values in any of the salts. The value for the S−F contacts was increased from 3.20 to 3.50 Å, reflecting the fact that the radius of sulfur is anisotropic.

(46) Valency units were calculated using Brown's relationship. The contacts of sulfur have been defined as $s = (R/R_0)^{-N}$ or $s = \exp[(R_0 - R)/B]$, where R is the observed distance, R_0 is the value of the bond length with the unit bond valence, and N and B are constants. The constants are available from http://ftp.ccp14.dl.ac.uk/ccp/web-mirrors/i_d_brown/bond_valence_param/ (Brown, I. D. *The Chemical Bond in Inorganic Chemistry—The Bond Valence Model*; Oxford University Press: Oxford, U.K., 2002).

(47) Gleiter, R. *Angew. Chem., Int. Ed.* **1981**, *20*, 444.

Table 2. Compilation of Structural Parameters and Pauling Bond Orders [a] of 7^{2+} in the MF_6^- (M = As, Sb) and $Sb_2F_{11}^-$ Salts

	$7(AsF_6)_2$[4a] (295 K)	$7(SbF_6)_2$ (173 K)	$7(Sb_2F_{11})_2$ (296 K)	$7(Sb_2F_{11})_2$ (123 K)
	Bond Distances (Å)/Pauling Bond Orders			
C−C	1.462(5)/0.99	1.471(6)/0.96	1.469(4)/0.97	1.475(6)/0.95
C−N	1.284(3)/1.83	1.281(7)/1.85	1.288(4)/1.80	1.291(6)/1.79
N−S1	1.600(2)/1.58	1.609(4)/1.53	1.601(3)/1.57	1.616(3)/1.50
S1−S2	2.070(1)/0.94	2.077(2)/0.92	2.062(2)/0.96	2.074(2)/0.93
S2−S3	2.018(1)/1.11	2.021(2)/1.10	2.014(2)/1.12	2.028(2)/1.07
C−S3	1.748(3)/1.26	1.746(5)/1.27	1.746(4)/1.27	1.747(5)/1.27
sum of the BOs in the ring	6.7	6.7	6.7	6.6
	Selected Angles (deg)			
C−C−N	120.3(2)	120.1(4)	119.5(2)	119.3(3)
C−N−S1	121.3(2)	120.8(4)	120.8(2)	120.7(3)
N−S1−S2	101.0(1)	101.2(2)	101.4(1)	101.2(2)
S1−S2−S3	97.5(4)	97.23(7)	97.53(5)	97.45(7)
S2−S3−C	96.8(9)	97.1(2)	97.0(1)	97.0(1)
S3−C−C	116.6(2)	116.2(3)	117.4(2)	117.1(3)

[a] Calculated using the following relation: $\log(BO) = (D_1 - D_n)/0.71$, where BO = bond order, D_1 = distance of a single bond [standard values (hybridization): C−C 1.46 (sp^2), C−N = 1.47 (sp^3), C−S = 1.82 (sp^3), N−S = 1.74 (sp^3), S−S = 2.05 (sp^3) Å], and D_n = observed bond distance.

Table 3. Valency Units[46] Calculated for the S···F Contacts in the Structures of $7(AsF_6)_2$, $7(SbF_6)_2$, and $7(Sb_2F_{11})_2$, Corresponding NBO Charges of 7^{2+} in Different Spin States and Calculated Spin Densities of the Triplet State of 7^{2+} [Calculated at the PBE0/6-31G* Level of Theory]

	valency units			NBO charges			
	$7(AsF_6)_2$	$7(SbF_6)_2$	$7(Sb_2F_{11})_2$	closed-shell singlet	open-shell singlet	triplet	spin density triplet
C				0.00	0.01	0.01	−0.01
N				−0.55	−0.56	−0.56	0.01
S1	0.31	0.32	0.38	0.85	0.77	0.78	0.30
S2	0.40	0.37	0.31	0.25	0.28	0.28	0.40
S3	0.27	0.22	0.31	0.45	0.50	0.50	0.30
total	0.98	0.91	1.00	1.00	1.00	1.00	1.00

Table 4. Calculated[a] and Experimental (X-ray) Bond Distances of 7^{2+}

		PBE0				CAS	
	$7(SbF_6)_2$	triplet[b]	open-shell singlet	closed-shell singlet	rotomer, triplet	triplet[b]	singlet
C−C	1.471(6)	1.469	1.470	1.445	1.485	1.472	1.474
C−N	1.281(7)	1.284	1.284	1.300	1.281	1.266	1.264
C−S3	1.746(5)	1.769	1.769	1.785	1.774	1.754	1.757
N−S1	1.609(4)	1.611	1.612	1.583	1.603	1.637	1.639
S1−S2	2.077(2)	2.108	2.108	2.086	2.119	2.044	2.044
S2−S3	2.021(2)	2.039	2.039	2.063	2.035	2.039	2.038

[a] Corresponding to fully optimized true minima. Bond distances calculated with the HF, B3LYP, and MPW1PW91 functionals are given in the Supporting Information. [b] Abbreviations PBE0 and CAS stand for PBE0/6-31G* and CASSCF[12,12]/6-311G* levels of theory, respectively.

supported by the results of an EPR study as well as magnetic susceptibility measurements of 7^{2+} "diluted" in a diamagnetic host (see sections 3.6 and 3.7).

Valence bond and molecular orbital (MO) descriptions of the structure of 7^{2+} predict that the sum of the bond orders within each $CNSSS^{\bullet+}$ ring should be 6.5 with five σ bonds, two π bonds, a nonbonding electron pair, and the seventh π electron in a π^* orbital. The sum of the calculated Pauling bond orders (Table 2) within the isolated ring is in general agreement with this description.

3.3.1. Packing Motifs of $7(MF_6)_2$ (M = As, Sb) and $7(Sb_2F_{11})_2$. The isomorphous $7(MF_6)_2$ structures contain alternating sheets of MF_6^- anions and planar 7^{2+} in the *bc* plane (see Figures 2a and S11 in the Supporting Information for more packing views), with each dication inclined at angles of 39.92(1)° [AsF_6^-] and 40.62(2)° [SbF_6^-] with respect to the *bc* plane. There are stacks of dications down the *a* and *b* axes, as illustrated in Figure 2a. The perpendicular distances between cations (with respect to the planes of the cations) within stacks along the *a* axis are 3.69(3) Å [AsF_6^-] and 3.50(3) Å [SbF_6^-]. The corresponding distances in the stacks along the *b* axis are 4.35(3) and 4.65(3) Å. The *a* stacks are slipped[48] (i.e., equivalent atoms in adjacent cations do not coincide with the normal of the plane of the cations) by 40.26(1) and 38.36(2)° and the *b* stacks by 34.63(3) and 36.04(3)° in AsF_6^- and SbF_6^- salts, respectively, in order to minimize the electrostatic repulsion between positively charged S atoms. The cation−cation contacts in the approximate plane through the plane of the cations (the angle between the approximate and actual planes of one particular cation is 5° in the AsF_6^- salt and 6° in the SbF_6^- salt)

(48) The slipping angle is defined as the angle between the normal of the plane through all atoms of one cation and the vector through one atom of the same cation and the equivalent atom in a neighboring cation in the stack.

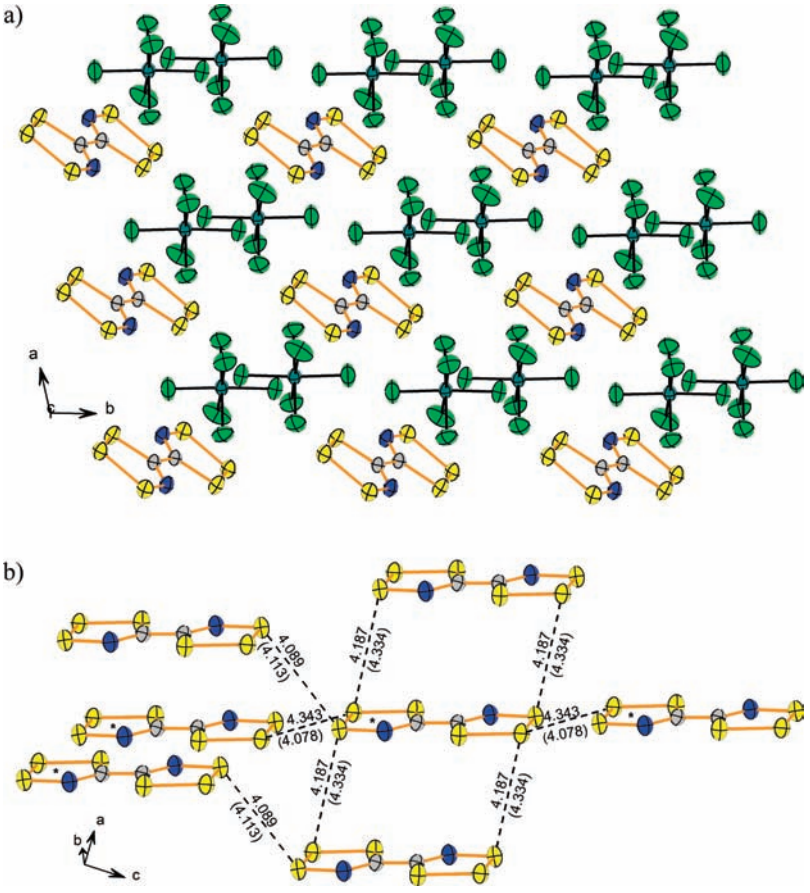

Figure 2. (a) Crystal packing of $\mathbf{7}(MF_6)_2$ (M = As, Sb) along the *c* axis showing alternating sheets of dications and anions lying in the *bc* plane. (b) $\mathbf{7}^{2+}$ *inter*layer and *inter*stack S−S dication contacts in $\mathbf{7}(MF_6)_2$ (MF_6^- anions have been removed for clarity). Values given for $\mathbf{7}(SbF_6)_2$ with those for $\mathbf{7}(AsF_6)_2$ in brackets (std. of S−S contacts, 0.002). Cations belonging to the same approximate plane through the plane of the cations are indicated with an asterisk. Thermal ellipsoids are drawn at 50% probability.

are shorter than those in the stack along the *a* axis for the AsF_6^- salt, while the opposite is true in the case of $\mathbf{7}(SbF_6)_2$ (see Figure 2b). This difference may be the origin of the dramatic difference seen in the magnetic properties of single crystals of these isostructural salts, which will be discussed in an upcoming paper.[21] Nonbonded radii, defined as twice the van der Waals radius of sp^2-hybridized sulfur perpendicular and parallel to the plane, are 4.06 and 3.20 Å, respectively.[49] The dications are therefore almost, but not completely, isolated from one another.

The packing in $\mathbf{7}(Sb_2F_{11})_2$ is similar to that of $\mathbf{7}(MF_6)_2$, but *inter*cationic distances are longer and the dications are more effectively separated by intervening anions (see Figure 3a). Note that the low-temperature structure is illustrated as the anion is ordered at −150 °C but becomes increasingly partially disordered upon an increase of the temperature (see the Supporting Information for further discussion). As shown in Figure 3a, the dications stack down the *a* axis inclined at an angle of 19.59(1)° to the *bc* plane with a slip angle of 54.93(2)°. However, there is no direct contact between cations in the stacks because the perpendicular distance between the planes of the dications is 6.90(2) Å and the closest distances between atoms in the neighboring cations in the stack are 7.250(5) Å for S(3)−N(1) and 7.282(2) Å for S(3)−S(3) (shown in Figure S12 in the Supporting Information and Figure 3b, respectively). The nearest *inter*cationic contacts are illustrated in Figure 3b, the shortest of which connect $\mathbf{7}^{2+}$ via S(3)−S(3) into a 1D strand. A discussion of temperature-dependent disorder of some of the $Sb_2F_{11}^-$ F atoms and the strength of the corresponding S···F contacts is given in the Supporting Information.

3.3.2. Are the Structures of the Red and Green 7-$(Sb_2F_{11})_2$ Crystals the Same? The red compound in all of the structures obtained at −150 to +73 °C has the same crystal packing, modified only by the increasing disorder of the F(8)−F(11) equatorial group around the Sb(2) atom (see Figure S12 in the Supporting Information). Thus, they all have the same structures with no phase change over the whole temperature range. The atomic parameters of the green compound from the structure determined at +23 °C are identical,[20] within experimental error, to those of the red compound also determined at +23 °C. Thus, all five structures represent the same crystal packing of the same ion pairs. However, some cautionary comments are included in the Supporting Information for those attempting to repeat the experimental work.

3.4. Vibrational Spectra of the Salts of $\mathbf{7}^{2+}$. The C_{2h} symmetry of $\mathbf{7}^{2+}$ leads to 12 IR-active and 12 Raman-active vibrational modes (mutually exclusive rule).[50] The actual spectra (Figures S2 and S3 in the Supporting Information) contain more than 24 peaks including the vibrational

(49) Nyburg, S. C.; Faerman, C. H. *Acta Crystallogr.* **1985**, *B41*, 274.

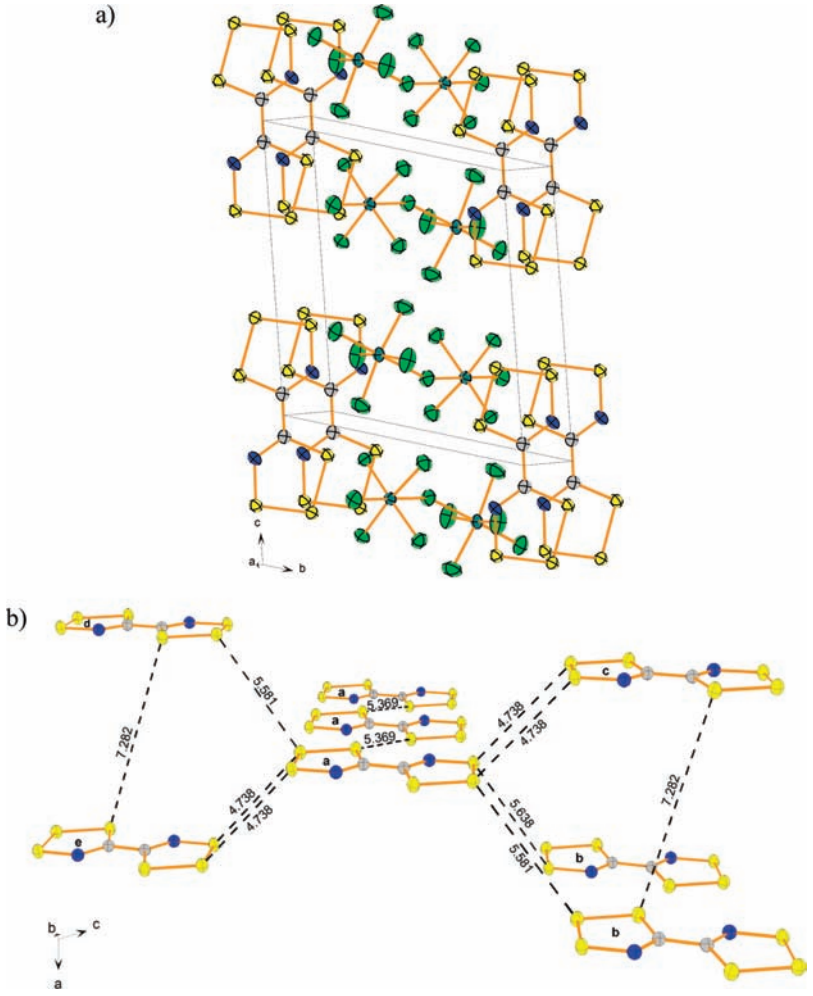

Figure 3. (a) Crystal packing view of $\mathbf{7}(Sb_2F_{11})_2$ (at −150 °C) along the *a* axis. (b) Illustration of the shortest S−S contacts between cations in $\mathbf{7}(Sb_2F_{11})_2$ (std. of S−S contacts, 0.002). Cations belonging to different strands are indicated with different letters (bold). Thermal ellipsoids are drawn at 50% probability.

modes of anions. The experimental and calculated vibrational frequencies of $\mathbf{7}^{2+}$ are in good agreement (Table 5). The assignment of calculated normal modes was carried out by a normal-coordinate analysis (see Tables S3 and S4 in the Supporting Information for details). The assignment shows that apart from the normal modes corresponding to the C=N and S−S stretching frequencies most of the normal modes involve several different internal coordinates, i.e., are mixed.

The C=N vibrational region is very complex, containing no less than nine vibrations between 1481 and 1607 cm^{-1} in the FT-Raman spectrum of $\mathbf{7}(AsF_6)_2$ at 120 K. The most intense Raman band at ca. 1510 cm^{-1} is attributed to the symmetric C=N vibration, and the weak bands between 1470 and 1490 cm^{-1} are attributed to the ^{13}C and ^{15}N isotopomers. Peaks at the higher wavenumbers could be due to overtones or combination bands. We note that peaks found above the region of the Raman-active C=N stretch are also observed in the FT-Raman spectra of $\mathbf{10}(AsF_6)_2$,[8] $\mathbf{10}(Sb_2F_{11})_2$, and **10**,[8] as well as in some $RCNS_3^{\bullet+}$ radical cations.[2] These features are likely an inherent property of CNS-containing five-membered heterocycles. The FT-Raman spectrum of $\mathbf{7}(Sb_2F_{11})_2$ in a SO_2 solution (see Figure S4 in the Supporting Information) does not show a similar pattern, but the peaks are much less intense than they are in the solid state. The room temperature FT-Raman spectra of the solids are less resolved than the spectra taken at 120 K but, nonetheless, contain the same features as those observed in the low-temperature spectra. This implies that the additional complexity of the vibrational spectra is likely not due to a phase change at low temperatures.

Although the ν_2 vibrational mode [1192 cm^{-1} in $\mathbf{7}(AsF_6)_2$] corresponding to C−C stretching shows some mixing with other internal coordinates, it clearly indicates that the C−C bond is closer to a single bond (cf. the *inter*-ring C−C stretch in biphenyl, 1275 cm^{-1})[51] than a double bond (e.g., C_2H_4, 1622.6 cm^{-1}).[52] Furthermore, comparison of the stretching force constants derived from calculated normal modes showed the C−C bond order to be 1.1 (see Supporting Information for details). In addition the bond orders for the S(1)−S(2) and S(2)−S(3) bonds were estimated using a stretching frequency bond order relationship developed earlier[53] and comparing calculated force constants. Both

(50) Nakamoto, K. *Infrared and Raman Spectra of Inorganic and Coordination compounds*, 4th ed.; Wiley-Interscience: Toronto, 1986.

(51) (a) Katon, J. E.; Lippincott, E. R. *Spectrochim. Acta* **1959**, 627. (b) Steele, D.; Lippincott, E. R. *J. Mol. Spectrosc.* **1961**, *6*, 238.

(52) Shimanouchi, T. *Tables of Molecular Vibrational Frequencies Consolidated Vol. I*; National Standards Reference Data Series 39; NBS: Washington, DC, 1972.

Table 5. Compilation of Experimental and Calculated [PBE0/6-31G*] Vibrational Frequencies of the Salts of $\mathbf{7}^{2+}$ [a]

$\mathbf{7}(AsF_6)_2$		$\mathbf{7}(SbF_6)_2$		$\mathbf{7}(Sb_2F_{11})_2$		calculated for $\mathbf{7}^{2+}$ [b]		
IR	Raman	IR	Raman	IR	Raman	triplet	BS singlet	assignments [c]
1624 (1)	1628 (1)	1620 (14)	1626 (1)	1634 (37)	1624 (1)			$2\nu_{18}$
	1581 (< 1)		1579 (< 1)					$\nu_{18} + \nu_{19}$
	1558 (2)		1558 (2)		1555 (2)			$\nu_3 + \nu_4$
	1542 (1)		1539 (1)		1537 (2)			$2\nu_{19}$
	1526 (sh)		1528 (sh)		1515 (sh)			$\nu_2 + \nu_8$
	1513 (100)		1514 (100)		1504 (100)	1608 (0/100)	1612 (0/100)	ν_1 [ν_s(C═N)]
1512 (5)		1515 (2)		1508 (6)		1614 (14/0)	1617 (14/0)	ν_{17} [ν_{as}(C═N)]
	1486 (< 1)		1484 (1)		1474 (1)			^{13}C isotopomer of ν_1
	1481 (< 1)							^{15}N isotopomer of ν_1
	1230 (1)		1231 (< 1)		1223 (< 1)			$2\nu_{20}$
	1192 (2)		1191 (2)		1186 (2)	1229 (0/9)	1224 (0/9)	ν_2 [mainly ν(C−C)[d]]
	911 (4)		908 (7)		909 (6)	937 (0/7)	933 (0/9)	ν_3 [mainly ν_s(S(1)−N)[d]]
	907 (4)				901 (2)			$\nu_1 - \nu_{20}$
811 (29)		810 (100)		810 (100)		836 (100/0)	836 (100/0)	ν_{18} [ν_{as}(S(1)−N)]
772 (14)		767 (40)		764 (9)		779 (68/0)	778 (68/0)	ν_{19} [mainly ν_{as}(S(3)−C)[d]]
	647 (2)		642 (2)		643 (< 1)	657 (0/1)	656 (0/1)	ν_4 [mixed ν_s(S(3)−C) and δ_s ring (ip)]
						650 (0/0)	650 (0/0)	ν_{14} [C−C bend (oop)]
626 (100)		627 (62)		625 (11)		638 (52/0)	637 (56/0)	ν_{20} [mixed δ_{as} ring (ip) and ν_{as}(S(3)−C)]
534 (2)	535 (3)	533 (1)		527 (4)		547 (4/0)	548 (4/0)	ν_{21} [ν_{as}(S(2)−S(3))]
	530 (3)		531 (1)		529 (2)	542 (0/2)	542 (0/2)	ν_5 [ν_s(S(2)−S(3))]
477 (3)		478 (15)		474 (61)		490 (12/0)	491 (12/0)	ν_{10} [mixed δ_s ring (oop) and C−C bend (oop)]
	464 (3)		459 (2)		468 (1)	441 (0/1)	438 (0/1)	ν_6 [mainly ν_s(S(1)−S(2)) [d]]
	457 (2)	447 (2)		454 (1)		436 (12/0)	437 (14/0)	ν_{22} [ν_{as}(S(1)−S(2))]
	418 (3)		416 (1)		417 (3)	430 (0/2)	430 (0/1)	ν_7 [mainly δ_s ring (ip)[d]]
372 s	373 (1)					404 (5/0)	404 (5/0)	ν_{23} [δ_{as} ring (ip)]
	335 (2)		337 (< 1)		335 (< 1)	334 (0/ > 1)	330 (0/1)	ν_8 [ρ ring (ip)]
	297 (< 1)		297 (< 1)			294 (0/ < 1)	293 (0/ < 1)	ν_{15} [δ_{as} ring (oop)]
	225 (1)		225 (1)			220 (0/ < 1)	219 (0/ < 1)	ν_9 (ring breathing)
						167 (6/0)	167 (6/0)	ν_{11} [δ_s ring (oop)]
						117 (0/0)	117 (0/0)	ν_{16} [δ_{as} ring (oop)]
						91 (3/0)	91 (3/0)	ν_{24} (ring scissoring)
						78 (2/0)	78 (2/0)	ν_{12} [C−C bend (oop)]
						48 (0/0)	45 (0/0)	ν_{13} (τ ring)

[a] Anion frequencies and assignments are included in Tables S5 and S6 in the Supporting Information. [b] Calculated intensities are listed as (IR/Raman), and the values are scaled to the most intense band in the spectrum, which is given a value of 100. Peak areas were approximated assuming triangular peaks and a flat baseline. [c] Abbreviations: sh, shoulder; ν, stretching; δ, deformation; τ, twisting; ρ, rocking; ip, in plane; oop, out of plane, s, symmetric; as, asymmetric; with respect to different rings of the cation. [d] Small contributions from other normal modes are not shown. See the Supporting Information for details.

methods gave estimated bond orders of 0.7 and 1.1 for the S(1)−S(2) and S(2)−S(3) bonds, respectively, which are in reasonable agreement with those calculated from bond distances (see Table 2).

The vibrational spectra of the anions were assigned by comparison to spectra of species where the anions have high symmetry, i.e., O_h symmetry for MF_6^- (M = As, Sb) and D_{4h} symmetry for *trans*-fluorine-bridged $Sb_2F_{11}^-$.[54] The observed spectra were more complex than the reference spectra, consistent with the lower symmetry of anions observed in the crystal structures of $\mathbf{7}^{2+}$ salts, e.g., approximate C_2 symmetry for the *cis*-fluorine-bridged $Sb_2F_{11}^-$. Details of the assignment of the anion frequencies are presented in the Supporting Information (Tables S5 and S6).

3.5. Computational and Theoretical Analysis of MOs and the Electronic Structure of $\mathbf{7}^{2+}$. Following Hoffmann's approach,[19] we constructed MOs of $\mathbf{7}^{2+}$ from the linear combination of the corresponding MOs of the $^{\bullet}CNSSS^{\bullet+}$ fragment, which can be formally derived from $\mathbf{7}^{2+}$ by breaking the C−C single bond. This generates an unpaired electron in the C σ orbital. By analogy with $C_5H_5^-$, the five constituent atoms of the $^{\bullet}CNSSS^{\bullet+}$ monomer give rise to five π MOs (designated as $\pi_1-\pi_5$ in Figure 4). However, the degeneracy of the π_2/π_3 (filled) and π_4/π_5 (empty) couples in $C_5H_5^-$ is lifted in $^{\bullet}CNSSS^{\bullet+}$ because of the differences in electronegativity and mismatch in energies of the constituent C, N, and S atoms. A similar MO description for bonding in the $CNSSS^+$ ring in the $HCNSSS^+$ derivative has been given previously at the ROHF/3-21G* level of theory.[1]

The two $^{\bullet}CNSSS^{\bullet+}$ monomers, each containing five π orbitals occupied by seven electrons, generate 10 π orbitals for $\mathbf{7}^{2+}$ (designated as $\Pi_1-\Pi_{10}$ in Figure 4). The nearly degenerate Π_7 and Π_8 (ΔE = 0.07 eV), which represent the two SOMOs of $\mathbf{7}^{2+}$, arise from a linear combination of the two half-filled π_4 orbitals of $^{\bullet}CNSSS^{\bullet+}$. Notably, the orbitals Π_7 and Π_8 are essentially nonbonding with respect to the C−C bond, thus accounting for the observed diradical nature of $\mathbf{7}^{2+}$.

The delocalized triplet-state SOMOs of $\mathbf{7}^{2+}$ are almost but not completely sulfur-based (sum of the SOMO S atom occupancies Π_7 0.94 and Π_8, 0.88; almost 100% of the calculated spin density on the S atoms; see Table 3) and equivalent to the localized SOMOs calculated using a symmetry-broken formalism (Figure 5). The SOMO atom occupancies give a picture similar to that of calculated spin densities (Table 3) but imply slightly

(53) Brownridge, S.; Cameron, T. S.; Du, H.; Knapp, C.; Köppe, R.; Passmore, J.; Rautiainen, J. M.; Schnöckel, H. *Inorg. Chem.* **2005**, *44*, 1660.
(54) (a) Begun, G. M.; Rutenberg, A. C. *Inorg. Chem.* **1967**, *6*, 2212. (b) Willner, H.; Schaebs, J.; Hwang, G.; Mistry, F.; Jones, R.; Trotter, J.; Aubke, F. *J. Am. Chem. Soc.* **1992**, *114*, 8972.

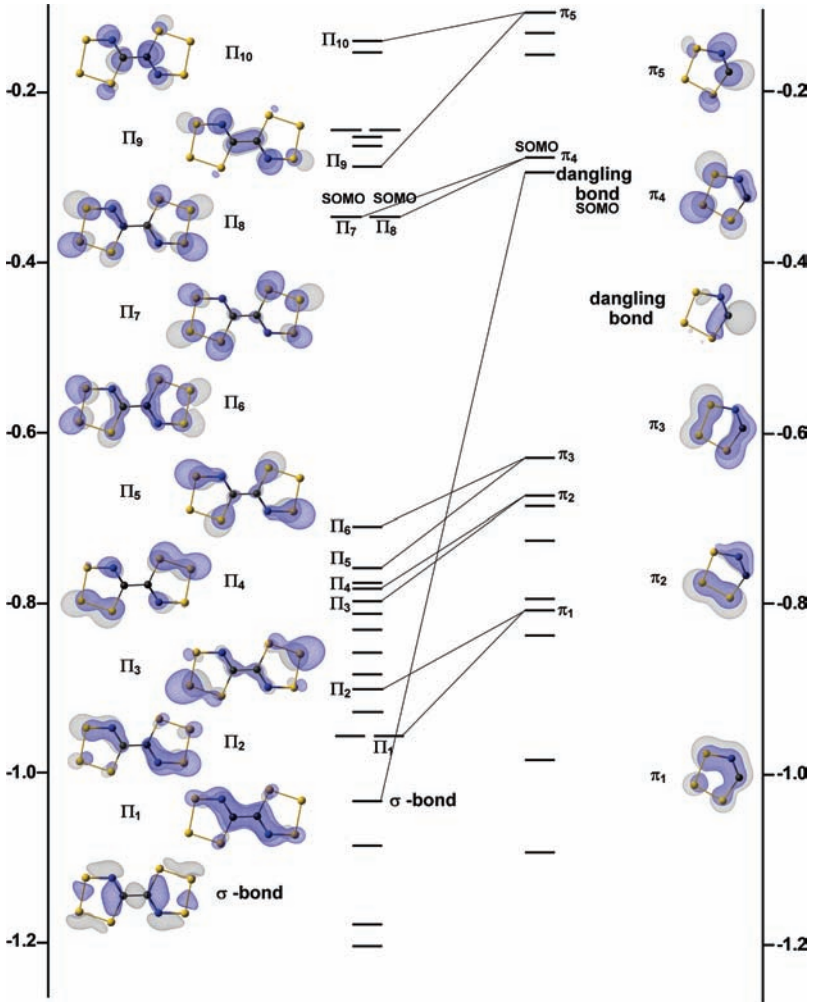

Figure 4. Diagram illustrating the formation of MOs of $^{\bullet+}$SSSNC−CNSSS$^{\bullet+}$ from the two $^{\bullet}$CNSSS$^{+\bullet}$ fragments. Note that π refers to the monomer-based π orbitals, while Π refers to the MOs of $\mathbf{7}^{2+}$; unlabeled orbitals are of the σ type. Monomer SOMOs refer to the unpaired electron on the π_4 orbital and in the dangling σ bond, respectively. Orbitals drawn at isosurface 0.05 au.

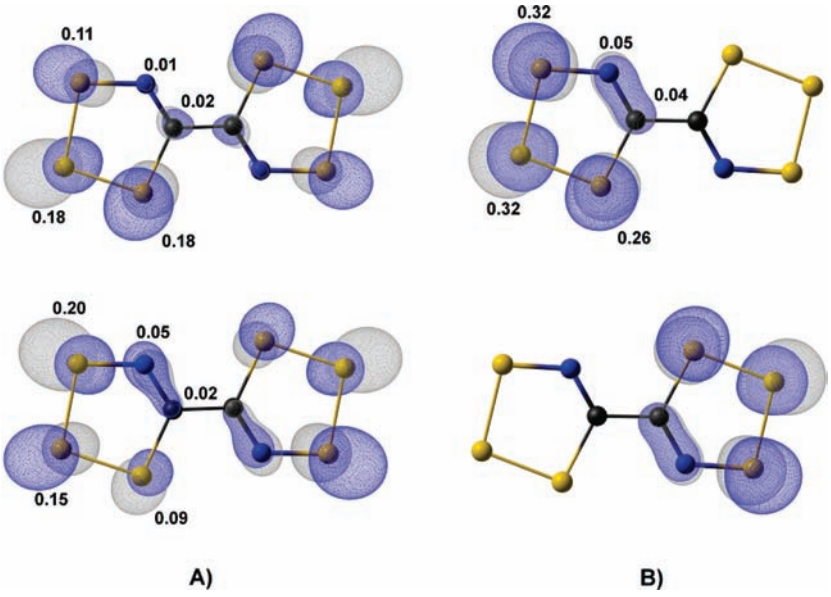

Figure 5. (A) Two SOMOs of the triplet state of $\mathbf{7}^{2+}$. (B) Two SOMOs for the symmetry-broken singlet state of $\mathbf{7}^{2+}$. Drawn at isosurface 0.05 au.

stronger interaction between the unpaired electrons (as indicated by the small occupancies on the C atoms). The spin-paired quinoidal structure $\mathbf{6}^{2+}$ (Chart 1) with a C═C double bond, which would have been expected

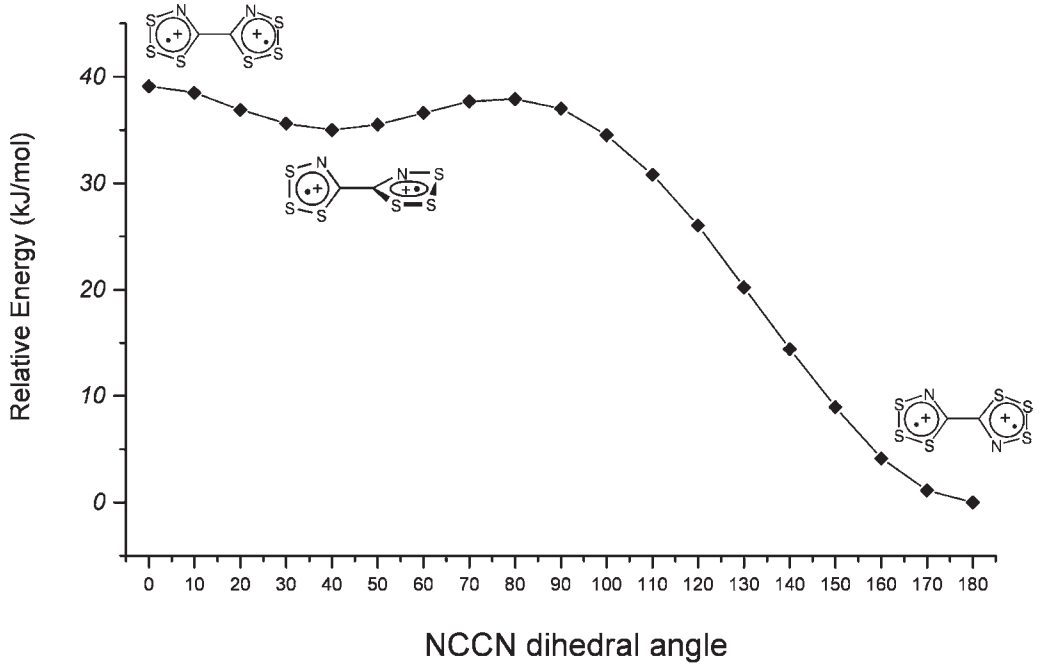

Figure 6. Calculated [PBE0/6-31G*] dependence of the energy of $\mathbf{7}^{2+}$ in its triplet state on the N−C−C−N dihedral angle between the two $-CNSSS^{\bullet+}$ rings.

based on a simple Lewis model, is not observed for $\mathbf{7}^{2+}$. The MO Π_9 represents the C−C π bond corresponding to the quinoidal structure. Depending on the energies of the nearly degenerate MOs Π_7 and Π_8 relative to that of Π_9, a diradical ground state, as in $\mathbf{7}^{2+}$, or a closed-shell singlet ground state, as in **11**−**14**, is observed. In the case of $\mathbf{7}^{2+}$, Π_9 lies much higher in energy (by about 1.56 eV). The geometry of the calculated closed-shell singlet (Table 4) is close to the triplet-state geometry. Thus, the closed-shell singlet corresponds to a double occupancy of the Π_7 orbital and not the quinoidal structure, which would be adopted if Π_9 were lower in energy than Π_7 and Π_8. No minimum corresponding to the quinoidal structure $\mathbf{6}^{2+}$ with a short C−C bond was found for $\mathbf{7}^{2+}$, in contrast to **10**,[8] where such a minimum was obtained. Partial optimization of $\mathbf{7}^{2+}$ by constraining the C−C bond to an approximate double-bond distance (1.334 Å) approximating the quinoidal structure gave a structure that was 99 kJ mol^{-1} higher in energy than the optimized $\mathbf{7}^{2+}$ structure (see Figure 11). The experimentally observed trans-planar geometry of the C_{2h} symmetry (with a 180° dihedral angle) that maximizes *intra*molecular $N^{\delta-}\cdots S^{\delta+}$ electrostatic interactions is the most stable conformation in the gas phase according to the results of the potential energy scan calculations about the C−C bond (Figure 6). However, there is a second minimum corresponding to ca. a 40° dihedral angle (C_2 symmetry) between the two rings. Both stationary points found at 180° and 40° are true minima, as indicated by the absence of imaginary frequencies. The cis conformation at 0°, with the two repulsive $S^{\delta+}\cdots S^{\delta+}$ and $N^{\delta-}\cdots N^{\delta-}$ interactions, can also be optimized; however, it is, in fact, a first-order saddle point, as indicated by the vibrational frequency analysis. In a SO_2 solution, a similar rotational profile of $\mathbf{7}^{2+}$ was calculated but with the barriers decreased by about 3 kJ mol^{-1}.

Table 6. Singlet−Triplet Gap ΔE_{ST} (cm^{-1})[a] of $\mathbf{7}^{2+}$ Calculated at the UPBE0 and CASPT2 Levels of Theory

	$\mathbf{7}^{2+}$
broken symmetry UPBE0	+125
CASPT2[8,8]	+217
CASPT2[12,12]	+264

[a] The positive sign of ΔE_{ST} means that the triplet state is the ground state (1 cm^{-1} = 1.1963 × 10^{-2} kJ mol^{-1}).

3.5.1. Theoretical Determination of the Ground State of $\mathbf{7}^{2+}$. The theoretical singlet−triplet gap of $\mathbf{7}^{2+}$ was determined using single-configuration broken-symmetry UPBE0 and multiconfiguration CASPT2 methods. The results are given in Table 6. All calculations assign the triplet state as the ground state of $\mathbf{7}^{2+}$. The calculated singlet−triplet gap is small (+217 and +264 cm^{-1} at the CASPT2[8,8] and CASPT2[12,12] levels, respectively). The calculated triplet ground state is consistent with the pseudo-disjoint nature of the highest occupied MOs Π_7 and Π_8. A comparison with related **8**−**10** neutral species (see Table S8 in the Supporting Information for results and discussion) showed singlet diradical ground states for **8** and **9** and only a very weak ferromagnetic coupling of electrons in **10**; i.e., theory predicts that $\mathbf{7}^{2+}$ is the most likely of these radicals to form a triplet state consistent with the experimental findings.[4,6−8] The calculation results are also consistent with the lack of features attributable to exchange interaction between radical centers in the EPR of **10**[8] and the onset of exchange interactions in the EPR spectrum of **8** observed at higher temperatures (303 K).[6b]

However, because of the relatively small singlet−triplet gap, the ground-state assignment of $\mathbf{7}^{2+}$ should be treated with some caution because CASPT2 calculations have been reported to have difficulty in accurately describing the singlet−triplet gaps of systems where the magnetic

electrons are only weakly coupled.[55] For an accurate description, even more rigorous methods are required, e.g., difference-dedicated configuration interaction calculations.[56] However, these calculations have not been attempted. Furthermore, it should be noted that, because of the similarities of the singlet- and triplet-state energies, the solid-state effects to the structures (e.g., dipole interactions from other ions) could influence the energy ordering of the states. This can lead to differences between theoretically determined and experimentally observed ground states. The experimental determination of the ground state of $\mathbf{7}^{2+}$ from magnetic measurements is presented in the following section.

3.6. Magnetic Properties of the Salts of $\mathbf{7}^{2+}$. Measurements at room temperature of the magnetic susceptibilities of the two salts of $\mathbf{7}(A)_2$ (A = AsF_6, SbF_6) show the essential paramagnetism of the diradical dication. The magnetic moment values at 300 K for $\mathbf{7}(A)_2$, where A = AsF_6 and SbF_6, are 2.36 and 2.51 μ_B, respectively, consistent with the presence of two unpaired electrons per dication and the disjoint nature of $\mathbf{7}^{2+}$ (theoretical μ_{eff} = 2.45 μ_B). Variable-temperature magnetic susceptibility studies on samples of $\mathbf{7}(A)_2$ (A = AsF_6, Sb_2F_{11})[4c] and on $\mathbf{7}(SbF_6)_2$, as reported here, give evidence for weak *anti*ferromagnetic exchange in the solid state in all three materials. Previously reported[20] variable-temperature susceptibility measurements of $\mathbf{7}(AsF_6)_2$ in a SO_2/AsF_5 solution obtained using Evan's method are consistent with the solid-state results given here.

Theoretical as well as experimental EPR studies, given elsewhere in this report, support the picture of a diradical in which the two electrons are, at most, very weakly coupled to each other within the molecular diradical unit. In an attempt to determine whether the apparent *anti*ferromagnetic behavior observed in the magnetic susceptibility studies of the $\mathbf{7}^{2+}$ salts arises from such *intra*molecular exchange, from *inter*molecular interactions in the crystal lattice, or both, magnetic susceptibility measurements were performed on a sample of $\mathbf{7}(Sb_2F_{11})_2$ doped into a diamagnetic host $\mathbf{10}(Sb_2F_{11})_2$. Significantly, this experiment was possible because $\mathbf{7}(Sb_2F_{11})_2$ is isomorphous with the diamagnetic material $\mathbf{10}(Sb_2F_{11})_2$. By diluting $\mathbf{7}^{2+}$ in a diamagnetic host, we aimed at eliminating any *inter*molecular interactions between dications to ensure that all variation of the magnetic susceptibility with temperature is due to *intra*molecular interactions. Both $\mathbf{7}(Sb_2F_{11})_2$ and $\mathbf{10}(Sb_2F_{11})_2$ contain dications that are next-but-one neighbors in the ionic array, weakly connected by two S···S [$\mathbf{7}(Sb_2F_{11})_2$] and S···N [$\mathbf{7}(Sb_2F_{11})_2$] interactions. Replacement of $\mathbf{10}^{2+}$ by $\mathbf{7}^{2+}$ would favor $\mathbf{7}^{2+}\cdots\mathbf{10}^{2+}$ interactions (S···S and S···N) rather than $\mathbf{7}^{2+}\cdots\mathbf{7}^{2+}$ (two S···S) interactions. Thus, $\mathbf{7}^{2+}\cdots\mathbf{7}^{2+}$ as neighbors is not favored and, on general statistical grounds, will lead to $\mathbf{7}^{2+}$ likely being homogeneously distributed in the host matrix of $\mathbf{10}(Sb_2F_{11})_2$. This is strongly supported by the single-crystal EPR studies that showed the material to contain essentially isolated $\mathbf{7}^{2+}$ dications.[4f]

(55) Queralt, N.; Taratiel, D.; de Graaf, C.; Caballol, R.; Cimiraglia, R.; Angeli, C. *J. Comput. Chem.* **2008**, *29*, 994.

(56) (a) Miralles, J.; Daudey, J.-P.; Caballol, R. *Chem. Phys. Lett.* **1992**, *198*, 555. (b) Miralles, J.; Castell, O.; Caballol, R.; Malrieu, J.-P. *Chem. Phys.* **1993**, *172*, 33.

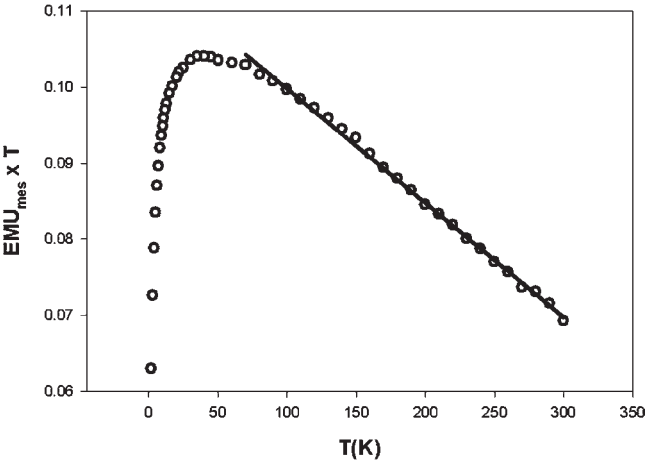

Figure 7. Measured signal times temperature ($EMU_{mes}T$) vs temperature plot for the dilute sample of $\mathbf{7}(Sb_2F_{11})_2$.

SQUID measurements were collected over the temperature range 2−300 K at an applied field of 10 000 G on a 0.1011 g sample of $\mathbf{7}(Sb_2F_{11})_2$ doped into $\mathbf{10}(Sb_2F_{11})_2$. A plot of the product of the measured signal (EMU_{mes}) times T versus T is shown in Figure 7. Analysis required that we first use the data to determine the weight fraction, f, of the diradical in the sample. This was accomplished by using the data obtained at temperatures above 70 K, where the plot is linear.

The linear portion above 70 K was analyzed as a straight line (solid line in Figure 7) with slope −0.000 149 9 (EMU) and intercept 0.1148 (EMU K). The overall measured signal is a composite of that due to the temperature-dependent paramagnetic signal from the diradical (EMU_{dirad}) and the temperature-independent diamagnetic signal from all atoms (EMU_{dia}) as well as any temperature-independent paramagnetic (TIP) signal present (EMU_{TIP}). Assuming that any exchange coupling between the electrons in the diradical is indeed small, as indicated earlier, and can be ignored above 70 K (the region of linearity of the graph), the intercept will correspond to $EMU_{dirad}T$ and the slope to $EMU_{dia} + EMU_{TIP}$. Magnetic susceptibilities for the diradical, χ_{dirad}, are obtained from

$$\chi_{dirad}T = (EMU_{dirad}TM_W)/(f \times \text{mass} \times H) \qquad (11)$$

where M_W is the molecular weight of $\mathbf{7}(Sb_2F_{11})_2$, f is its mass fraction in the doped sample, and H is the applied field. Employing the value 0.7505 as the $\chi_{dirad}T$ value for two unpaired and uncoupled electrons yields 0.174 for the value of f.

At all temperatures over the range 2−300 K, the value of EMU_{dirad} can be obtained from

$$EMU_{dirad} = EMU_{mes} - (-0.0001499) \qquad (12)$$

Employing eq 12 with a value 0.174 for f, the values of χ_{dirad} can be calculated for all temperatures, as can μ_{eff} values for the diradical.

For curve-fitting purposes, we halved the χ_{dirad} values obtained above for the doped sample to obtain values for the monoradicals, $\chi_{monorad}$ and, hence, μ_{eff} values for the monoradicals. These are plotted as a function of the

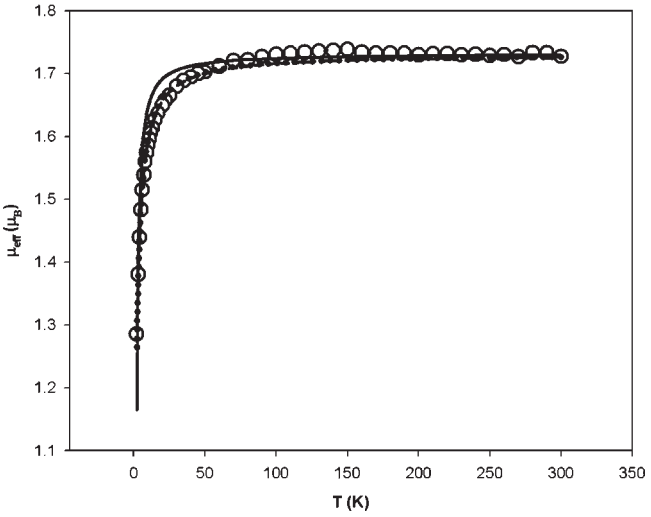

Figure 8. μ_{eff} vs T plot for the dilute sample of $\mathbf{7}(Sb_2F_{11})_2$.

temperature in Figure 8. The decrease in the moment observed at low temperatures suggests some form of *anti*ferromagnetic interaction. We analyzed the susceptibility data employing the Bleany−Bowers equation[31] in which J is the *intra*molecular coupling constant and g was set at 2.00 in all analyses presented here. Allowing J to vary produced the best fit, shown as the solid line in the figure, for a value of $J = -1.23\ cm^{-1}$. Visual inspection shows that this analysis fails to reproduce the general shape of the experimental curve at low temperatures. In spite of the fact that *inter*molecular interactions are anticipated to be negligible in a dilute sample, we analyzed the susceptibility data by employing the Bleany−Bowers equation in a form that includes, in addition to J for *intra*molecular exchange, a Weiss θ term (employing the $T-\theta$ form of the Curie−Weiss law) to allow for *inter*molecular exchange. Allowing both J and θ to vary and plotting the best-fit curve as the magnetic moment versus temperature gave the dashed line shown in Figure 8 for values of $J = +0.56\ cm^{-1}$ and $\theta = -2.29$ K. The agreement between the theory and experiment is much improved in this case. An equally good fit is obtained assuming simple Curie−Weiss behavior. This is shown as a dotted line in Figure 8, where θ has the best-fit value of −1.77 K. For the diluted sample, we conclude that, while there is measurable overall *anti*ferromagnetic exchange present, it is extremely weak. Importantly, for this study, the magnitude of *intra*molecular exchange in the $\mathbf{7}^{2+}$ dication, as measured by J, is small with $|J| < 1\ cm^{-1}$. The results are not inconsistent with the presence of a diradical species in which there is, at most, a small separation between the singlet and triplet states, a situation suggested elsewhere in this report by EPR and theoretical calculations.

In our earlier communication, we analyzed the magnetic susceptibility data obtained for nondiluted samples of $\mathbf{7}(AsF_6)_2$ and $\mathbf{7}(Sb_2F_{11})_2$ using the Bleany−Bowers equation for pairs of interacting $S = {}^1/_2$ magnetic centers.[4c] This yielded rather poor fits; importantly though, the study led to the conclusion that, at most, only very weak *anti*ferromagnetic exchange was present in the two compounds, with the strength of the exchange being much weaker in the latter. In Figure 9, measured mag-

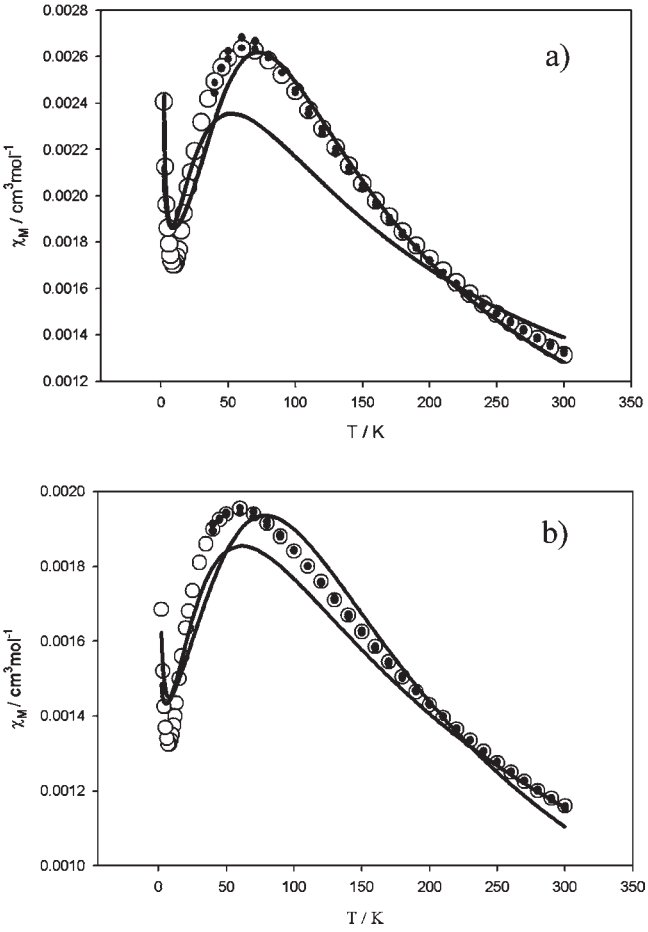

Figure 9. Temperature dependence of χ of (a) $\mathbf{7}(SbF_6)_2$ and (b) $\mathbf{7}(AsF_6)_2$. Open circles present experimental data, and lines indicate theoretical fits (see text). In all cases, values of χ are quoted per radical center (i.e., half a diradical). Fitting parameters are given in Table 7.

netic susceptibilities (on a per monoradical basis, i.e., $\chi_{monoradical}$ as described above) are plotted versus T for $\mathbf{7}(SbF_6)_2$ and $\mathbf{7}(AsF_6)_2$ (data for $\mathbf{7}(Sb_2F_{11})_2$ are presented in Figure S13 in the Supporting Information). The data are new for $\mathbf{7}(SbF_6)_2$ and those published earlier[4c] for $\mathbf{7}(AsF_6)_2$ [and $\mathbf{7}(Sb_2F_{11})_2$]. The earlier analysis of the data for the AsF_6^- and $Sb_2F_{11}^-$ salts, employing the Bleany−Bowers equation, is not appropriate given the study described above on the diluted sample of $\mathbf{7}^{2+}$ that revealed that *intra*molecular exchange is negligible. In the present work, we analyze the data for these salts as well as the new data for the SbF_6^- salt under the assumption that *intra*molecular exchange can be ignored.

For $\mathbf{7}(AsF_6)_2$ and $\mathbf{7}(SbF_6)_2$, the presence of broad maxima in the susceptibility (at ca. 60 K) suggests a low-dimensional nature of magnetic *inter*molecular interactions between diradical centers. Accordingly, we have examined fits of the data for these salts to two published models for *anti*ferromagnetic exchange interactions in extended systems: one for infinite 1D chains, which we will term the Hall model,[32] and the other for infinite 2D sheets, termed the Lines model[33] here. It is important to note that, whereas the Hamiltonian employed in the Hall model takes the form $\mathcal{H} = 2J\sum S_i \cdot S_j$, that for the Lines model is of the form $\mathcal{H} = J\sum S_i \cdot S_j$. Hence, a direct comparison of the J values between the models requires

Table 7. Fitted Magnetic Parameters[a] for $\mathbf{7}(SbF_6)_2$ and $\mathbf{7}(AsF_6)_2$

	$\mathbf{7}(SbF_6)_2$				$\mathbf{7}(AsF_6)_2$			
	Hall		Lines		Hall		Lines	
	2−300 K	40−300 K	2−300 K	40−300 K	2−300 K	40−300 K	2−300 K	40−300 K
$\lvert J\rvert/cm^{-1}$	31.6(0.9)	32.2(0.1)	51.4(2)	40.7(0.3)	42.0(1)	45.0(0.1)	61.8(1)	57.2(0.1)
θ/K	14(2)	4.1(0.3)	−15(1)	8(1)	1(3)	−25.9(0.6)	−20(1)	−15.6(0.3)
TIP/10^6 cm^{-1}	194(29)	266(2)	447(37)	278(7)	112(30)	240(3)	268(23)	242(2)
% P[b]	0.2 (0.04)	0 (fixed)	0 (fixed)	0 (fixed)	0.07 (0.04)	0 (fixed)	0 (fixed)	0 (fixed)

[a] g was fixed at 2.0 for all analyses. The numbers shown in brackets are standard deviations. [b] % P values were fixed at zero for all 40−300 K data analyses and for some 2−300 K data analyses where inclusion generated unrealistic negative values.

that the Lines J values be halved. The equations given for these two models were both modified slightly to include a contribution to the susceptibility from TIP and a Weiss θ to allow for any additional interactions that may be indicated, in addition to those measured by J in the models. The susceptibility data for these salts show a sharp increase on cooling below approximately 20 K because of, we conclude, paramagnetic impurity. Accordingly, the equations were also modified to include a fraction P of paramagnetic impurity, itself modeled as a simple $S = {}^1/_2$, $g = 2.0$ component. "Fits" of the experimental susceptibility values to calculated values, over the temperature range 2−300 K, were examined for both salts using both models, and the resulting "best fits" are shown in Figure 9a,b as solid black lines for the Hall model and solid gray lines for the Lines model. The corresponding fit parameters are given in Table 7. In the curve fitting done in this study, the value of g was fixed at 2.0, consistent with the EPR studies reported herein. While the calculated curves generally follow the trend of the experimental data, clearly the "fit" is not good in any of the cases. In particular, it is difficult to model the relatively sharp decline in the susceptibility at temperatures just below the maximum as well as the relatively sharp increase in the susceptibility observed upon cooling at the lowest temperatures. Accordingly, we focused our attention on the temperature region from just below the susceptibility maximum to room temperature (40−300 K), a region where the effects of paramagnetic impurities are minimized. In each of these analyses, the value of P was fixed at zero. The best-fit calculated susceptibilities are shown as filled circles in the figures, filled black for the Hall model fit and gray for the Lines model fit. The corresponding best-fit parameters are given in Table 7. We now examine the 40−300 K fits for $\mathbf{7}(AsF_6)_2$ and $\mathbf{7}(SbF_6)_2$ in detail and consider the significance of the parameter values generated in this process.

The 40−300 K data for $\mathbf{7}(SbF_6)_2$ are modeled best over this temperature range by the 1D-chain Hall model. The 2D-sheet Lines model does not produce the experimental data well near the susceptibility maximum. In both cases, the fitting required the inclusion of a Weiss θ parameter of 4.1 K for the Hall fit and 8 K for the Lines fit. This parameter serves to account for any factors, such as additional magnetic interactions, not specifically modeled. For example, in the analysis of the data using the Hall model, the magnetic behavior of the compound can be described as following, approximately, that of an extended chain of $S = {}^1/_2$ spins, *anti*ferromagnetically coupled with a coupling strength corresponding to $|J| = 32.2\ cm^{-1}$. Deviation from pure single-chain behavior is measured by the Weiss constant θ of 4.1 K. In effect, the smaller the θ is, the closer the behavior is to that of isolated chains. This analysis suggests that there are higher-dimensional interactions than 1D in the compound. The fit to the 2D Lines model is actually slightly worse, suggesting that this is not modeling the data and that the magnetic properties of $\mathbf{7}(SbF_6)_2$ are best described as consistent with the presence of *anti*ferromagnetically coupled chains with additional, weaker, *inter*chain interactions. The presence of multiple pathways for exchange coupling is not unexpected given the complex extended molecular structure exhibited by this compound. It should be noted too that the θ value of 4.1 K ($2.85\ cm^{-1}$), which is taken as a measure of the secondary interactions, generated in the Hall fit, is an order of magnitude weaker than the primary *intra*chain interactions as measured by $|J| = 32.2\ cm^{-1}$. This supports the conclusion that the Hall model is providing a reasonable description of the magnetic properties of the compound. In the case of the Lines model fit, the θ value of 8 K ($5.56\ cm^{-1}$) is proportionally larger in comparison to $|J|$, consistent with the conclusion that this model is inappropriate.

The 40−300 K data for $\mathbf{7}(AsF_6)_2$ are reproduced reasonably well by both the 1D and 2D models, although the quality of the fit is slightly better for the 2D Lines model in this case. Importantly, however, the θ "correction" factor is substantial in both instances (Table 7), indicating that neither model is providing an appropriate description of the exchange interactions in the compound. We conclude that in the case of $\mathbf{7}(AsF_6)_2$ no particular chain or sheet pathway dominates.

Calculated DFT coupling constants support (see the Supporting Information for details) the 1D chain model for magnetic behavior of $\mathbf{7}(SbF_6)_2$, consistent with the magnetic data analysis. Although the magnetic analysis was inconclusive regarding the dimensionality of the exchange of $\mathbf{7}(AsF_6)_2$, the DFT calculations support 2D behavior. Calculations suggest that the cation stacks in both salts form an important *anti*ferromagnetic pathway. In addition to *intra*stack interaction, $\mathbf{7}(AsF_6)_2$ appears to exhibit significant *inter*stack *anti*ferromagnetic interaction (via 4.113 Å S···S contact; see Figure 2b).

An analysis of the analogous $\mathbf{7}(Sb_2F_{11})_2$ data (given in the Supporting Information) shows the presence of only weak *anti*ferromagnetic coupling (an order of magnitude smaller than that observed for the other two salts) consistent with the much larger *inter*cationic contacts.

Table 8. Experimental Spin-Hamiltonian Parameters of $\mathbf{7}(Sb_2F_{11})_2$ Doped in a Crystal of $\mathbf{10}(Sb_2F_{11})_2$[4f] and Simulated Spin-Hamiltonian Parameters of $\mathbf{7}(AsF_6)_2$ in a Frozen SO_2/AsF_5 Solution[4c,d]

	g principal values			*D* principal values		
	xx	*yy*	*zz*	*xx*	*yy*	*zz*
single crystal[4f]	2.017 082	2.002 206	2.027 133	177.00	218.03	−395.03
				$D = -592.5 \pm 2.9$; $E = 20.5 \pm 2.0$ MHz		
frozen solution[4c,d]	2.0096	1.9943	2.0210	$D = -555$; $E = 54$ MHz (solution 1)[a]		
	2.0198	1.9844	2.0211	$D = -555$; $E = 22$ MHz (solution 2)[a]		

[a] Two different solutions gave almost identical simulated spectra, both in good agreement with the experimentally observed spectrum. The results for solution 2 are in slightly better agreement with those of the single crystal.

In summary, variable-temperature (2−300 K) magnetic susceptibility studies on a sample of $\mathbf{7}(Sb_2F_{11})_2$ doped into the isomorphous diamagnetic host material, $\mathbf{10}(Sb_2F_{11})_2$, revealed that the magnitude of *intra*molecular exchange in the $\mathbf{7}^{2+}$ dication, as measured by *J*, is small, with $|J| < 1\ cm^{-1}$ corresponding to a singlet−triplet gap of $< \pm 2\ cm^{-1}$. The overall *anti*ferromagnetic behaviors observed for nondiluted samples of the $\mathbf{7}(A)_2$ salts, as evidenced by decreasing moments with temperature in all three salts and the appearance of susceptibility maxima near 60 K in the MF_6^- (M = As, Sb) salts, arise mostly from *inter*molecular exchange interactions. Attempts to quantify the magnitude of the exchange interactions and establish the dimensionality of exchange in $\mathbf{7}(MF_6)_2$ by fitting the susceptibility data to known magnetic models for *anti*ferromagnetic exchange in 1D-chain and 2D-sheet extended systems were partly successful. Analyzing the 40−300 K data for $\mathbf{7}(SbF_6)_2$ gave the best fit for the 1D model with $|J| = 32\ cm^{-1}$. Importantly, however, while $\mathbf{7}(SbF_6)_2$ shows dominant 1D-chain behavior, the necessity of including a small θ value in the analysis suggests the existence of additional exchange pathway(s). In the case of $\mathbf{7}(AsF_6)_2$, magnetic modeling attempts showed the neither 1D nor 2D models were appropriate for the compound, suggesting the existence of complex exchange pathways where no particular one dominates.

3.7. EPR Spectra of $\mathbf{7}(MF_6)_2$ (M = As, Sb) and $\mathbf{7}(Sb_2F_{11})_2$. The EPR spectra of $\mathbf{7}(AsF_6)_2$, $\mathbf{7}(SbF_6)_2$, and $\mathbf{7}(Sb_2F_{11})_2$ in a SO_2/MF_5 solution (M = As, Sb) were measured at +20, −80, and −160 °C (frozen solution). The spectra of $\mathbf{7}(AsF_6)_2$ are given in Figure 1 of ref 4c and compared with those of the other similar salts in the Supporting Information (Figures S14−S16). The simulated EPR parameters obtained for the frozen-solution spectra of $\mathbf{7}(AsF_6)_2$[4c,d] and those for $\mathbf{7}(Sb_2F_{11})_2$ in a host single crystal of $\mathbf{10}(Sb_2F_{11})_2$[4f] are given in Table 8.

The solution EPR spectra of all three salts contain two resonances: a narrow resonance superimposed onto a broader peak with essentially identical *g* values [$\mathbf{7}(AsF_6)_2$, 2.0162; $\mathbf{7}(SbF_6)_2$, 2.0127; $\mathbf{7}(Sb_2F_{11})_2$, 2.0143], none of which shows any ^{14}N hyperfine splitting, and the *g* values, peak widths, and intensities vary significantly from one salt to another. The broader of the two resonances is attributed to the triplet state ($S = 1$) of $\mathbf{7}^{2+}$. The observation of the triplet state in solution is characteristic of diradicals with weakly coupled electrons.[57]

Freezing the solutions to −160 °C causes the broader of the two resonances to split into six zero-field-splitting components, and an additional resonance is observed at half-field ($\Delta m_s = \pm 2$), confirming the presence of triplet-state species (see Figure S17 in the Supporting Information). The frozen-solution spectra of the three salts of $\mathbf{7}^{2+}$ have very similar spectroscopic features, with the separation between the outermost splitting lines corresponding to *D* (the axial zero-field-splitting parameter, a measure of the effect of the magnetic field of one unpaired electron onto another) of 555 ± 10 MHz. The spectra were simulated by two similar sets of data,[4c,d] and the principal values of *g* were typical of a 7π radical, in which g_{min} ($= g_{yy}$) is just less than g_e and is perpendicular to the molecular plane (Figure 10). The largest component of the dipole tensor D_{zz} lies in the molecular plane, and assuming a point dipole approximation, we calculated the separation between "point electrons" as ca. 5.2 Å,[58] which is in good agreement with quantum-chemical calculations that place almost all of the spin density on S atoms (Table 3). The small value of *D* is consistent with very weak coupling between the unpaired spins and a very small singlet−triplet energy gap, conforming to the variable-temperature magnetic susceptibility measurements and the quantum-chemical calculations.

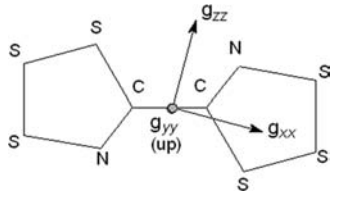

Figure 10. Orientations of *g* components with respect to the plane of the molecule.

The parameters extracted from single-crystal EPR measurements[4f] (Table 8) are in better agreement with the corresponding parameters of the frozen solution 2 than those of solution 1. Notably, the value of g_{yy} is very close to that of the free spin, as expected for a π radical with the unpaired electron in a p_π orbital perpendicular to the plane of the molecule. Therefore, the description of $\mathbf{7}^{2+}$ as a diradical with two weakly interacting unpaired electrons is consistent with the observed EPR spectra.

The origin of the narrower resonance located in the middle of the solution EPR spectra (see Figures S14−S16 in the Supporting Information) is controversial. The width of this resonance is unaffected by differences in the MF_5 (M = As, Sb) concentration, suggesting that it arises from a doublet species ($S = {}^1/_2$), in which relaxations are less

(57) Atherton, N. M. *Electron Spin Resonance: Theory and Applications*; Wiley: New York, 1973.

(58) The distance between the two spin centers has been calculated by $R_0 = (0.65g^2/D)^{1/3}$.

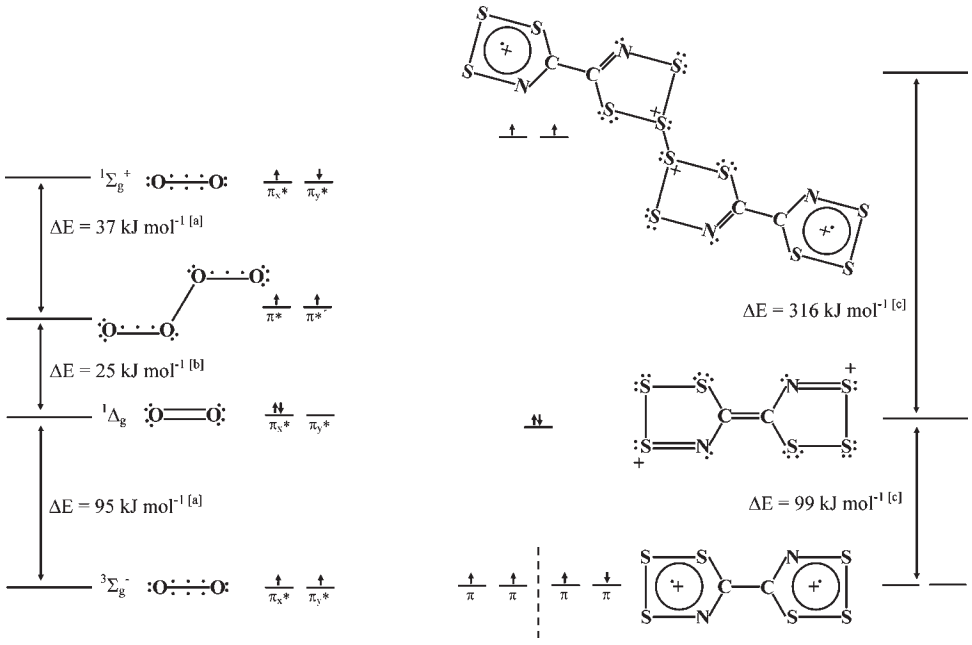

Figure 11. Comparison of the electronic states of O_2 and planar $\mathbf{7}^{2+}$.[62] Structures of $(O_2)_2$, quinoidal $\mathbf{7}^{2+}$, and a dimer of $\mathbf{7}^{2+}$ have been obtained by partial optimization by constraining the middle O−O bond (1.50 Å), the C=C bond (1.334 Å), and the *intra*dimer S−S bond (2.10 Å), respectively.[63] Energy differences are given per monomer. The three electron bond descriptions for oxygen have been adopted from ref 64: [a] experimental energies from ref 65; [b] calculated at the CCSD(t)/6-311G* level: [c] calculated at the PBE0/6-311G* level.

drastically affected by the solvent.[57] However, it seems unlikely that it arises from a reduced species, e.g., $\mathbf{7}^{\bullet+}$, because of the presence of an excess of oxidizing agent (see section 3.2). The *g* values of the broad and narrow resonances are essentially identical (within experimental error), implying that the two arise from species with very similar structures. The high purity of $\mathbf{7}(AsF_6)_2$ (elemental analysis and vibrational spectra) precludes the presence of an impurity giving rise to such an intense signal. It also has to be noted that the EPR spectrum of a single crystal of $\mathbf{7}(Sb_2F_{11})_2$ doped into $\mathbf{10}(Sb_2F_{11})_2$ did not contain such a narrow resonance. Previously, the narrower resonance in solution spectra of $\mathbf{7}^{2+}$ was proposed to arise from a metastable rotomer obtained by rotation about the C−C single bond.[4c,d] Indeed, such a rotomer was found in the gas phase as a minimum corresponding to the twisted conformation with a N−C−C−N dihedral angle of 40° (Figure 6). The π-orbital overlap in the rotomer would be minimal because of breaking of the coplanarity of the rings and an increased distance between unpaired spins, leading to an EPR spectrum of a doublet state rather than a triplet state. However, the calculated energy difference of ca. 33 kJ mol^{-1} (30 kJ mol^{-1} in a SO_2 solution; Figure 6) implies that a significant population of this rotomer conformation is unlikely. Careful simulations of all observed solution EPR spectra did not reveal any correlation between the ratios of triplet and singlet states and the temperature. Instead, these ratios seemed to depend more on the anion. It is possible that $\mathbf{7}^{2+}$ forms an ion pair $\mathbf{7}^{2+}\cdots MF_6^-/Sb_2F_{11}^-$ with $S^{\delta+}\cdots F^{\delta-}$ interactions that replace the $S^{\delta+}\cdots N^{\delta-}$ contacts in the planar conformation and stabilize the rotomer configuration. As noted above, the ring rotation likely leads to decoupling of the unpaired electrons in $\mathbf{7}^{2+}$. Interestingly, many of the published EPR spectra of triplets in the literature also contain an additional narrow resonance in the center, but satisfying explanations are rarely given. The most common proposal is that the sharp central resonance is due to monoradical impurities;[13b,d,59] however, in our case, the $S = {}^1/_2$ monoradical $\mathbf{7}^{\bullet+}$ can be excluded in the presence of an excess of oxidizing agent MF_5. The radical trication $\mathbf{7}^{3+}$ could be a possibility, but our quantum-chemical calculations [MPW1PW91/6-31G*] predict that the oxidation of $\mathbf{7}^{2+}$ to $\mathbf{7}^{3+}$ by AsF_5 is endothermic by about 2479 kJ mol^{-1} in the gas phase, and experimental attempts to prepare $\mathbf{7}^{3+}$ failed. In some cases in the literature, an alternative explanation of the central peak was an isomeric diradical form[13c] or chemical exchange-narrowing effects.[60] In our situation, the origin of the narrow resonance is most likely due to a rotomer $\mathbf{7}^{2+}$ stabilized by ion-pairing effects. All salts of $\mathbf{7}^{2+}$ dissolve in SO_2, AsF_3, SO_2/MF_5, and $AsF_3/SO_2/MF_5$ mixtures to give green solutions. It is likely that this green color is due to the $\mathbf{7}^{2+}$/anion ion pair. The green surface of the red $\mathbf{7}(Sb_2F_{11})_2$ could arise from this or a related $\mathbf{7}^{2+}/Sb_2F_{11}^-$ ion pair. However, the origin of the green color in the crystals of $\mathbf{7}(Sb_2F_{11})_2$ remains an open question.

4. Conclusions and Comparison of $\mathbf{7}^{2+}$ with O_2

The reaction of NC−CN with a 1:1 mixture of $S_4(MF_6)_2$ and $S_8(MF_6)_2$ (M = As, Sb) (stoichiometrically equivalent to four "S_3MF_6" units) results in the quantitative formation of red $\mathbf{7}(MF_6)_2$ (eqs 2 and 7) in one-step reactions. Other stoichiometries also resulted in the formation of $\mathbf{7}^{2+}$, the thermodynamically favored product in this reaction. $\mathbf{7}(Sb_2F_{11})_2$ was

(59) Selected examples: (a) Spagnol, G.; Shiraishi, K.; Rajca, S.; Rajca, A. *Chem. Commun.* **2005**, 5047. (b) Sato, K.; Sawai, T.; Shiomi, D.; Takui, T.; Wang, Q.; Wang, J.-S.; Li, Y.; Wu, G.-S. *Synth. Met.* **2003**, *137*, 1197. (c) Rajca, A.; Rajca, S.; Wongsriratanakul, J. *Chem. Commun.* **2000**, 1021. (d) Bushby, R. J.; McGill, D. R.; Ng, K. M.; Taylor, N. *J. Chem. Soc., Perkin Trans. 2* **1997**, 1405.

(60) Ziessel, R.; Stroh, C.; Heise, H.; Köhler, F. H.; Turek, P.; Claiser, N.; Souhassou, M.; Lecomte, C. *J. A. Chem. Soc.* **2004**, *126*, 12604.

prepared by the reaction of $\mathbf{7}(AsF_6)_2$ with an excess SbF_5. $\mathbf{7}(AsF_6)_2$ and $\mathbf{7}(Sb_2F_{11})_2$ gave excellent elemental analyses, while $\mathbf{7}(SbF_6)_2$ contained some diamagnetic $(SbF_3)_3SbF_5$. All salts were characterized by X-ray structure determinations, rigorous assignment of vibrational spectra including a normal-coordinate analysis, variable-temperature magnetic susceptibility measurements, and EPR spectroscopy. Evidence was presented for $\mathbf{7}^+$ given by the reduction of $\mathbf{7}(AsF_6)_2$ in liquid SO_2. $\mathbf{7}^{2+}$ was also investigated by several theoretical methods. The X-ray structures of red $\mathbf{7}(Sb_2F_{11})_2$ and green $\mathbf{7}(Sb_2F_{11})_2$ previously reported as different[4e,20] have been shown to likely be the same. All results show that $\mathbf{7}^{2+}$ contains two $CNSSS^{\bullet+}$ radical cations joined by a single C−C bond in a trans-planar *centro*symmetric arrangement due to *intra*cationic electrostatic $N^{\delta-}\cdots S^{\delta+}$ interactions. EPR studies in solution give a broad peak that we attribute to the triplet-state $\mathbf{7}^{2+}$ in equilibrium with a sharp singlet peak, which is likely a $\mathbf{7}^{2+}$ rotomer/anion ion pair. Our previous EPR studies[4f] of single crystals of $\mathbf{7}(Sb_2F_{11})_2$ diluted in isomorphous diamagnetic host $\mathbf{10}(Sb_2F_{11})_2$ unambiguously demonstrated $\mathbf{7}^{2+}$ to exhibit a triplet state arising from interaction of the unpaired electrons in p_π orbitals (largely sulfur) in each of the rings (see Figures 5 and 11). In this work, we report that variable-temperature magnetic studies on this material give an energy difference between the open-shell singlet and triplet states of less than ± 2 cm^{-1}; i.e., they are essentially degenerate. Therefore, $\mathbf{7}^{2+}$ can be seen to be similar to O_2 in that they are both triplet-state molecules and do not adopt classical electron-paired structures of quinoidal $\mathbf{6}^{2+}$ and singlet $^1\Delta_g$ O_2, which are about 100 kJ mol^{-1} higher in energy (see Figure 11). The higher energy of the $\mathbf{6}^{2+}$ isomer is attributed to the loss in π bond energy[61] and positive charge localization relative to $\mathbf{7}^{2+}$. In contrast to $\mathbf{7}^{2+}$, with essentially degenerate open-shell singlet and triplet states, the unpaired electrons of O_2 are strongly coupled and the observed singlet state of O_2 lies much higher in energy than the O_2 triplet state (see Figure 11). Furthermore, the unpaired electrons in O_2 and $\mathbf{7}^{2+}$ do not pair in the solid state to form chemically bonded dimers or polymers. Figure 11 illustrates the energetically unfavorable formation of dimers of O_2 and $\mathbf{7}^{2+}$. Dimerization of O_2 results in the loss of a strong π bond (352 kJ mol^{-1}) and the gain of a weaker σ bond (142 kJ mol^{-1}).[44] Dimerization of $\mathbf{7}^{2+}$ can be regarded to occur with the loss of a S−S π bond (199 kJ mol^{-1}) and the gain of the related σ bond of similar strength (226 kJ mol^{-1}) but is strongly disfavored by electrostatic repulsion and positive charge localization in the dimer. At very low temperatures, the magnetic susceptibilities of both solid O_2[5] and salts of $\mathbf{7}^{2+}$ decrease because of *anti*ferromagnetic *inter*molecular coupling of unpaired electrons. For salts of $\mathbf{7}^{2+}$, *anti*ferromagnetic *inter*molecular coupling decreases with an increase in the size of the anion, and we note that different structural forms of O_2 have different magnetic properties.[5] Thus, there are significant similarities between O_2 and $\mathbf{7}^{2+}$ in the gas phase and in its various salts. Notwithstanding some definite differences, i.e., unpaired electrons are parallel to one another and very weakly coupled in $\mathbf{7}^{2+}$, whereas those in O_2 are perpendicular and strongly coupled, $\mathbf{7}^{2+}$ has an isomeric rotomer that cannot exist for O_2, $\mathbf{7}^{2+}$ can be said to be O_2-like even though it is sulfur-based. It is the first example of an essentially sulfur-based diradical, as evidenced by calculated spin densities. As far as we are aware, O_2 and the salts of $\mathbf{7}^{2+}$ are the only simple nonsterically hindered main-group isolated compounds to show paramagnetism in the solid state. In this paper, we focused on the molecular properties of $\mathbf{7}^{2+}$ and its relationship to O_2. Further studies on intriguing variable-temperature magnetic and other bulk physical properties of single crystals of $\mathbf{7}(MF_6)_2$ are in progress.[21]

Acknowledgment. We thank the Natural Sciences and Engineering Research Council (NSERC) of Canada for funding (T.S.C. and J.P.), the Alexander von Humboldt Foundation in Germany for providing a Feodor−Lynen Fellowship (C.K.), the Ministry of Education in Finland and Helsingin Sanomat Foundation for providing financial support (J.M.R.), Dr. Sandra Altmannshofer and Prof. Dr. Wolfgang Scherer, University of Augsburg, Augsburg, Germany, for unpublished crystallographic data on $\mathbf{7}(SbF_6)_2$, Prof. Dr. Scherer and Dr. Ernst-Wilhelm Scheidt (Augsburg) for helpful comments on the interpretation of the magnetic data, Dr. Scott Brownridge for the FT-Raman measurements, Rod McGregor for collaboration with EPR spectroscopy, Dr. Gilles Villemure for assistance with UV/vis spectroscopy, and Dr. Heikki Tuononen, University of Jyväskylä, Jyväskylä, Finland, for his help with the MCSCF calculations and normal-coordinate analysis.

Supporting Information Available: X-ray crystallographic data in CIF format for $\mathbf{7}(SbF_6)_2$ and $\mathbf{7}(Sb_2F_{11})_2$ at different temperatures, UV/vis spectrum of $\mathbf{7}(AsF_6)_2$ in a SO_2/AsF_5 solution, FT-Raman and IR spectra of $\mathbf{7}^{2+}$ species, results of normal-coordinate analysis of $\mathbf{7}^{2+}$, assignment of anionic vibrational frequencies, predicted and observed coordination in $\mathbf{7}^{2+}$ salts, packing of $\mathbf{7}(MF_6)_2$ (M = As, Sb), structural depictions of anions in $\mathbf{7}^{2+}$ salts, cautionary comments on the effect that the measurement temperature has on observed reduced cell parameters of $\mathbf{7}(Sb_2F_{11})_2$, relation of disorder in $Sb_2F_{11}^-$ to the S···F contact strength and temperature, in situ EPR spectrum of the reduction of $\mathbf{7}(AsF_6)_2$ with $Na_2S_2O_4$ in SO_2, EPR spectra of $\mathbf{7}^{2+}$ salts in a SO_2/AsF_5 solution, magnetic susceptibility data of $\mathbf{7}^{2+}$ salts, discussion on the magnetic properties of $\mathbf{7}(Sb_2F_{11})_2$, optimized structural parameters of $\mathbf{7}^{2+}$ at different levels of theory, comparison of lowest states of $\mathbf{7}^{2+}$ with related main-group radicals, and calculated magnetic coupling pathways in crystals of $\mathbf{7}^{2+}$ salts. This material is available free of charge via the Internet at http://pubs.acs.org.

(61) Sum of the π bond energies in observed delocalized geometry: $2E(C{=}N) + 2E(S{=}S) = 2 \times 322 + 2 \times 152 = 949$ kJ mol^{-1}. Sum of the π bond energies in the quinoidal structure: $E(C{=}C) + 2E(N{=}S) = 266 + 2 \times 204 = 674$ kJ mol^{-1}. Thus, the observed structure is favored by 274 kJ mol^{-1} with respect to the quinoidal structure based on π bond energies and further stabilized by resonance and charge delocalization. Bond energies are taken from ref 44.

(62) Note that there is also a rotomer of $\mathbf{7}^{2+}$ that has been observed in equilibrium with the planar triplet state $\mathbf{7}^{2+}$ in solution.

(63) The partially optimized structure of $\mathbf{7}^{2+}$ is only a rough approximation of a true quinoidal structure because the strength of the C−N bonding tends to make the C−N bonds shorter than normal C−N single bonds and, in turn, the S−N bonds longer than double bonds.

(64) Pauling, L. *The Nature of the Chemical Bond*, 3rd ed.; Cornell University: Ithaca, NY, 1960.

(65) Herzberg, G. *Spectra of Diatomic Molecules*; Van Nostrand Reinhold: New York, 1950.